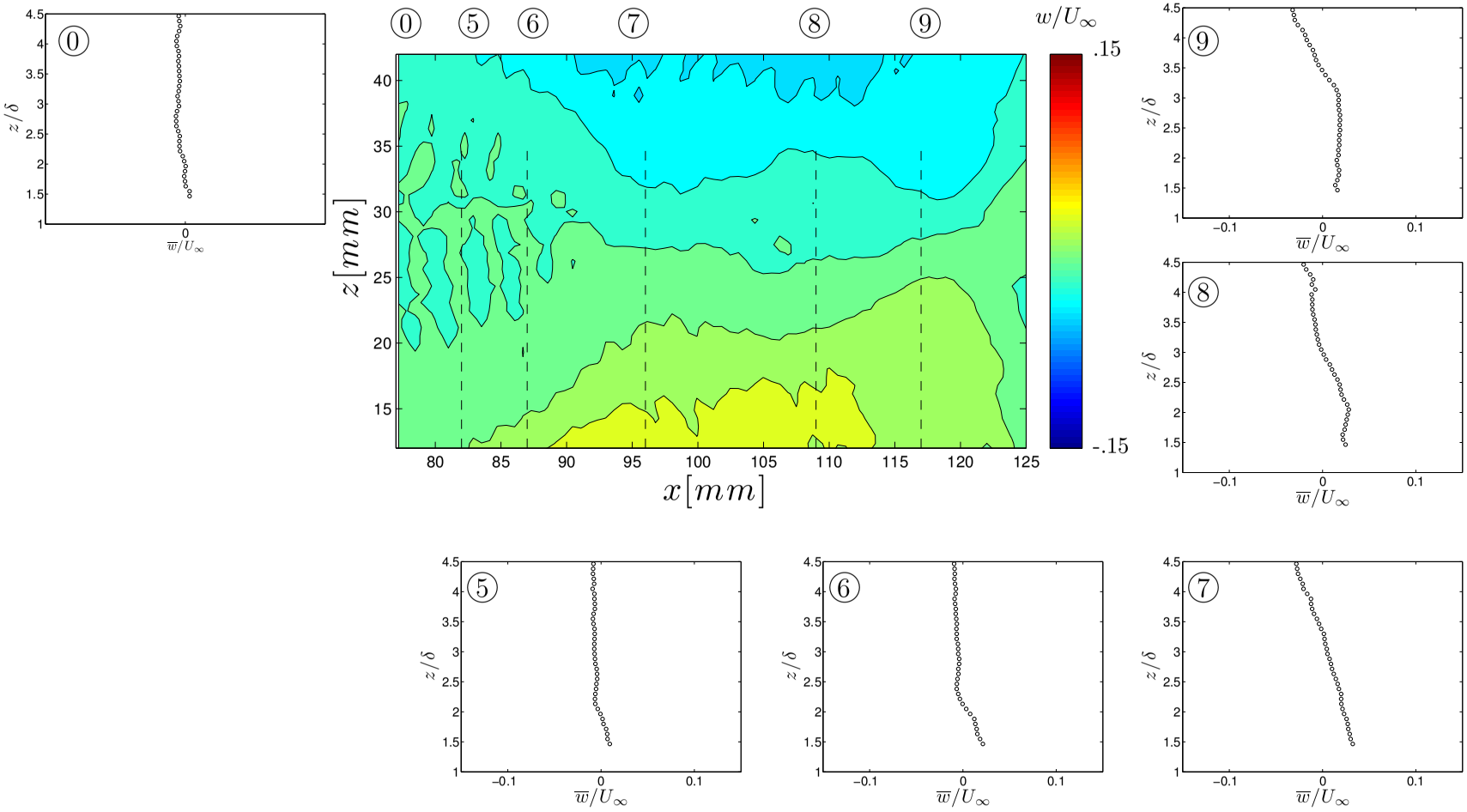

Figure C.11: Evolution of $\overline{w}$ through the y=1.9mm SBLI region for a flow deflection angle of $\theta = 6$ deg. Sampling numbers correspond to transverse plane sampling locations, location '0' indicating the region where U_∞ was calculated. At top, colors show the $\overline{w}$ field throughout each sampling plane, and also indicate their relative locations.

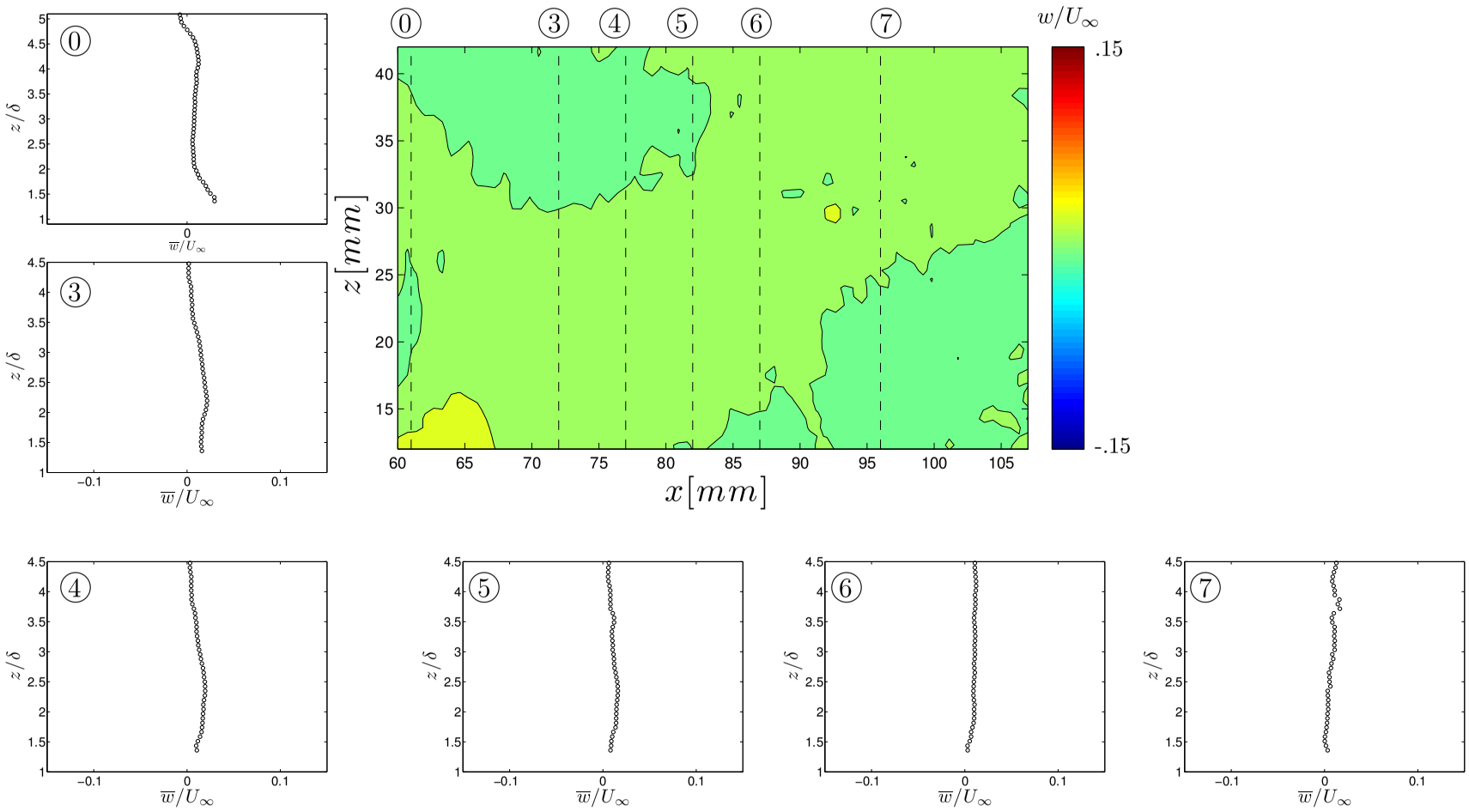

Figure C.12: Evolution of $\overline{w}$ through the y=2.85mm SBLI region for a flow deflection angle of $\theta = 6$ deg. Sampling numbers correspond to transverse plane sampling locations, location '0' indicating the region where U_∞ was calculated. At top, colors show the $\overline{w}$ field throughout each sampling plane, and also indicate their relative locations.

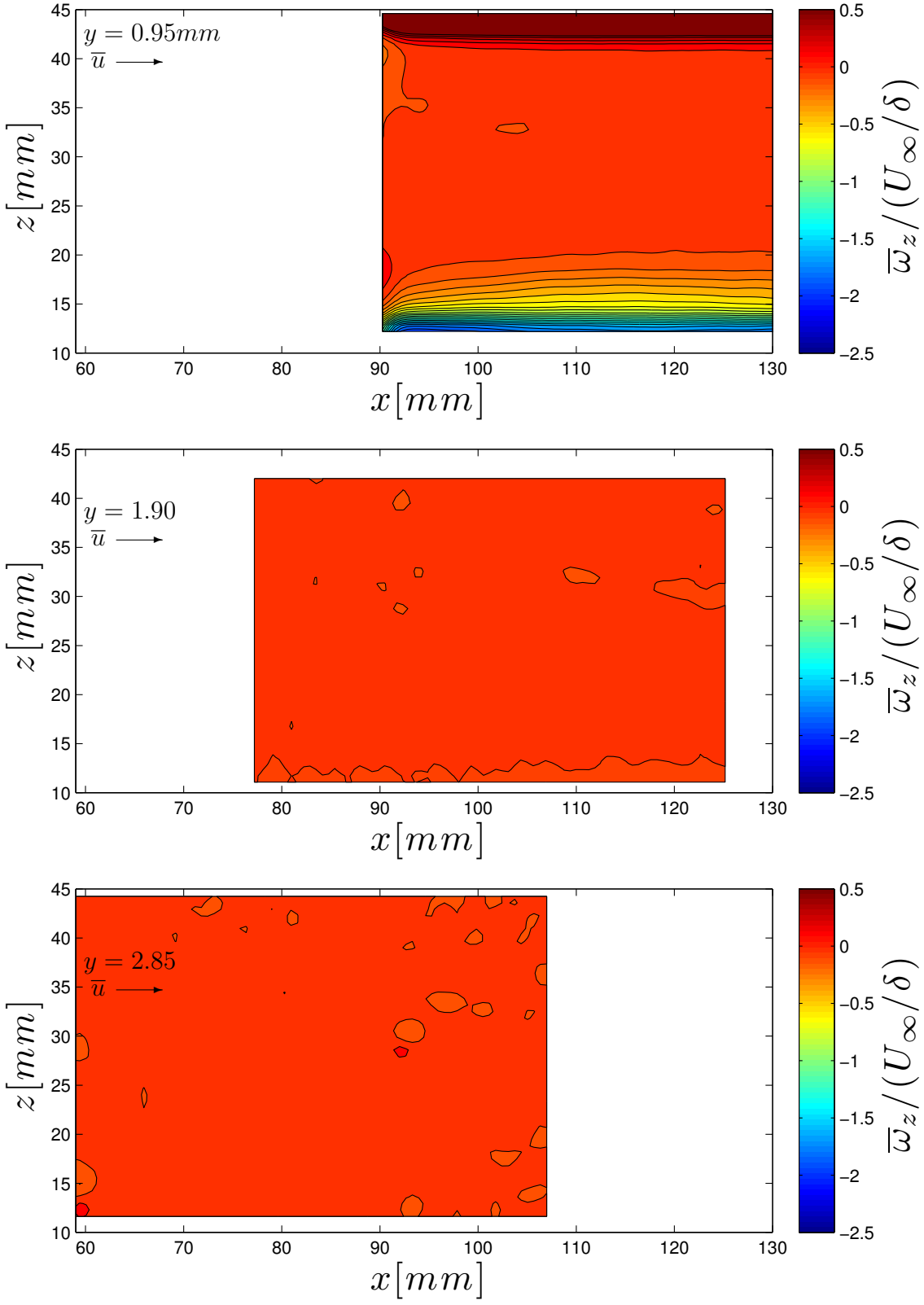

Figure C.13: Visualizations of the velocity component $\overline{\omega}_y$ for each of the three horizontal planes oriented in the streamwise direction.

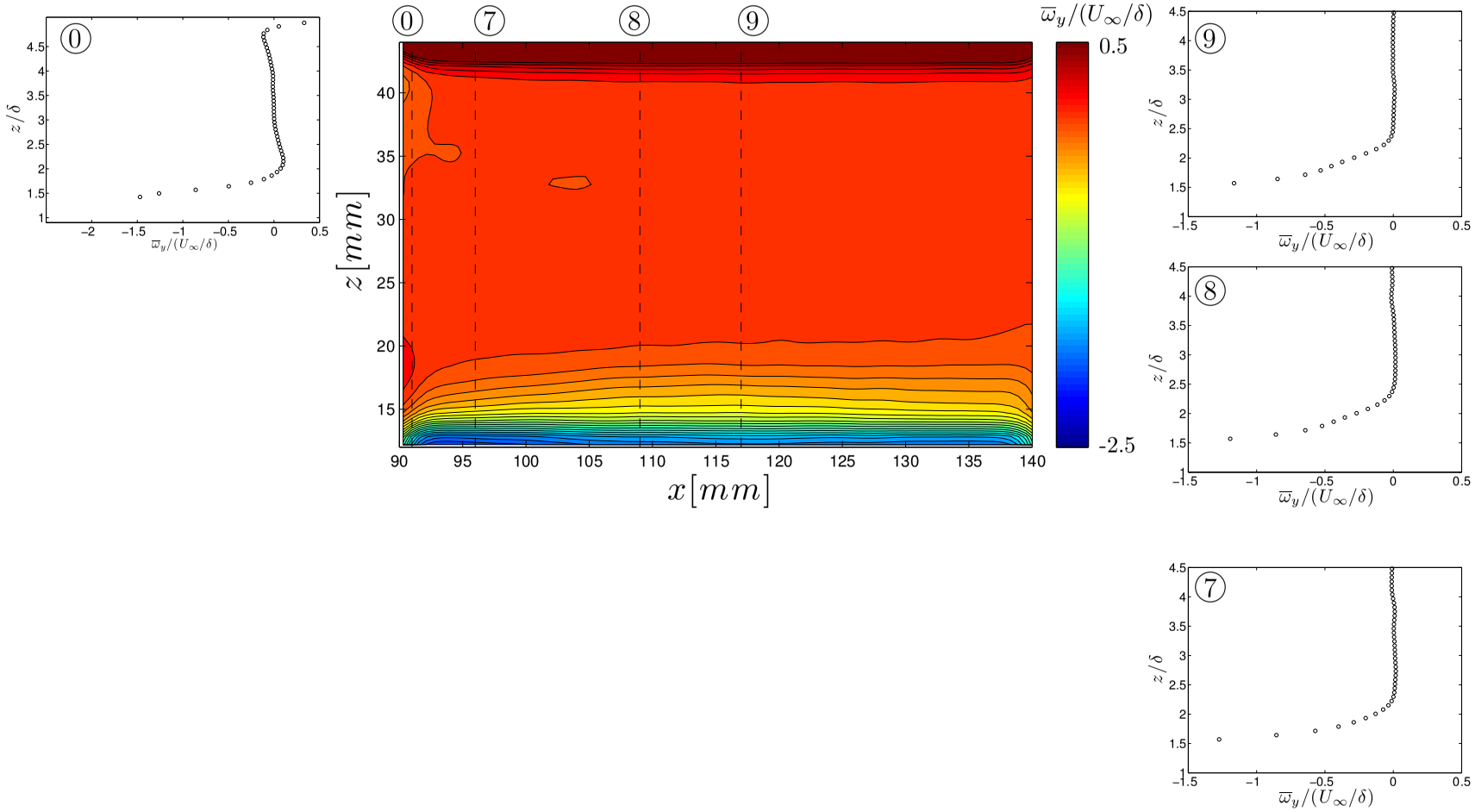

Figure C.14: Evolution of $\overline{\omega}_y/(U_\infty/\delta)$ through the y=9.5mm SBLI region for a flow deflection angle of $\theta = 6$–deg. Sampling numbers correspond to transverse plane sampling locations, location '0' indicating the region where U_∞ is calculated. At top, colors show the $\overline{\omega}_y/(U_\infty/\delta)$ field throughout each sampling plane, and also indicate their relative locations.

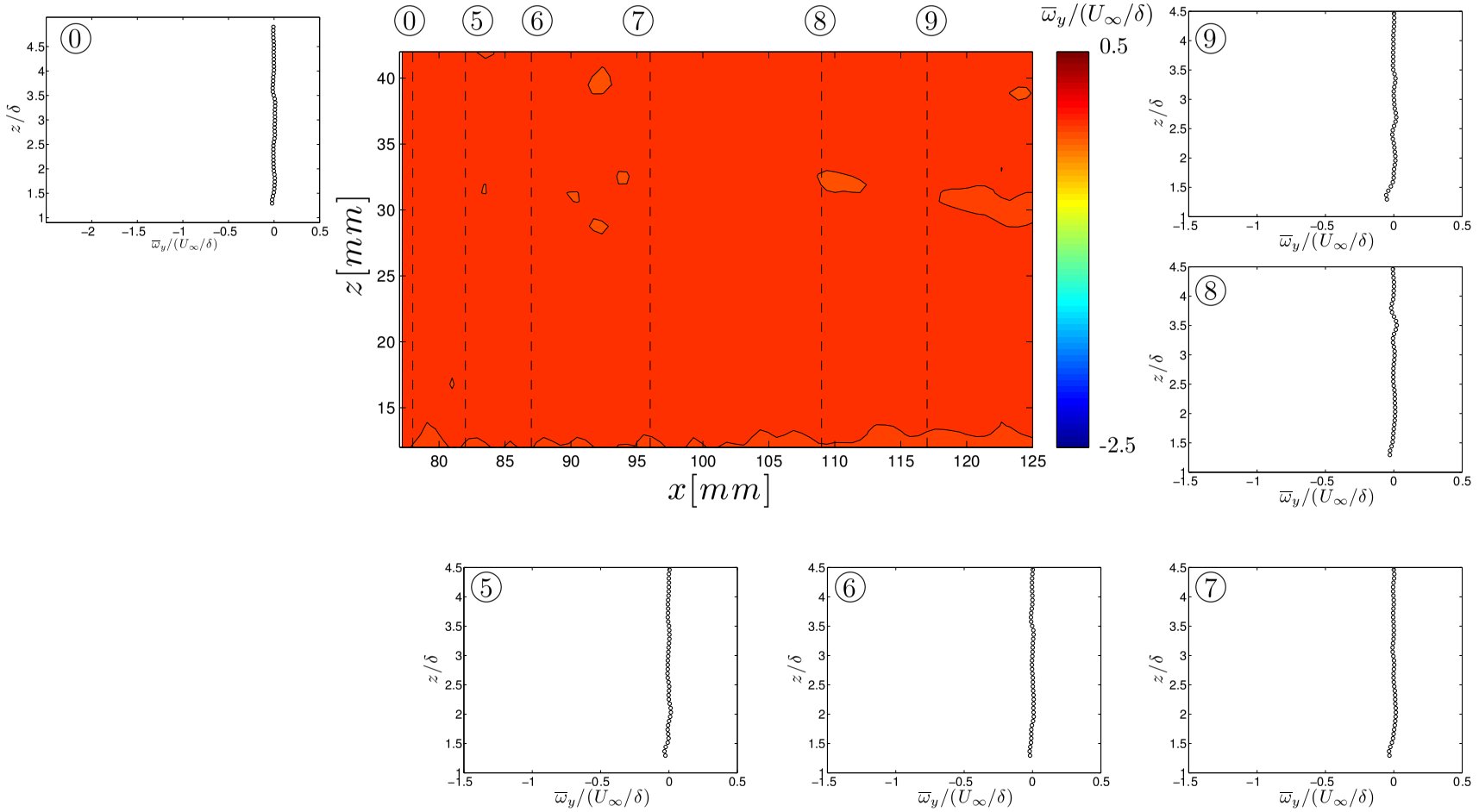

Figure C.15: Evolution of $\overline{\omega}_y/(U_\infty/\delta)$ through the y=19mm SBLI region for a flow deflection angle of $\theta = 6$ deg. Sampling numbers correspond to transverse plane sampling locations, location '0' indicating the region where U_∞ was calculated. At top, colors show the $\overline{\omega}_y/(U_\infty/\delta)$ field throughout each sampling plane, and also indicate their relative locations.

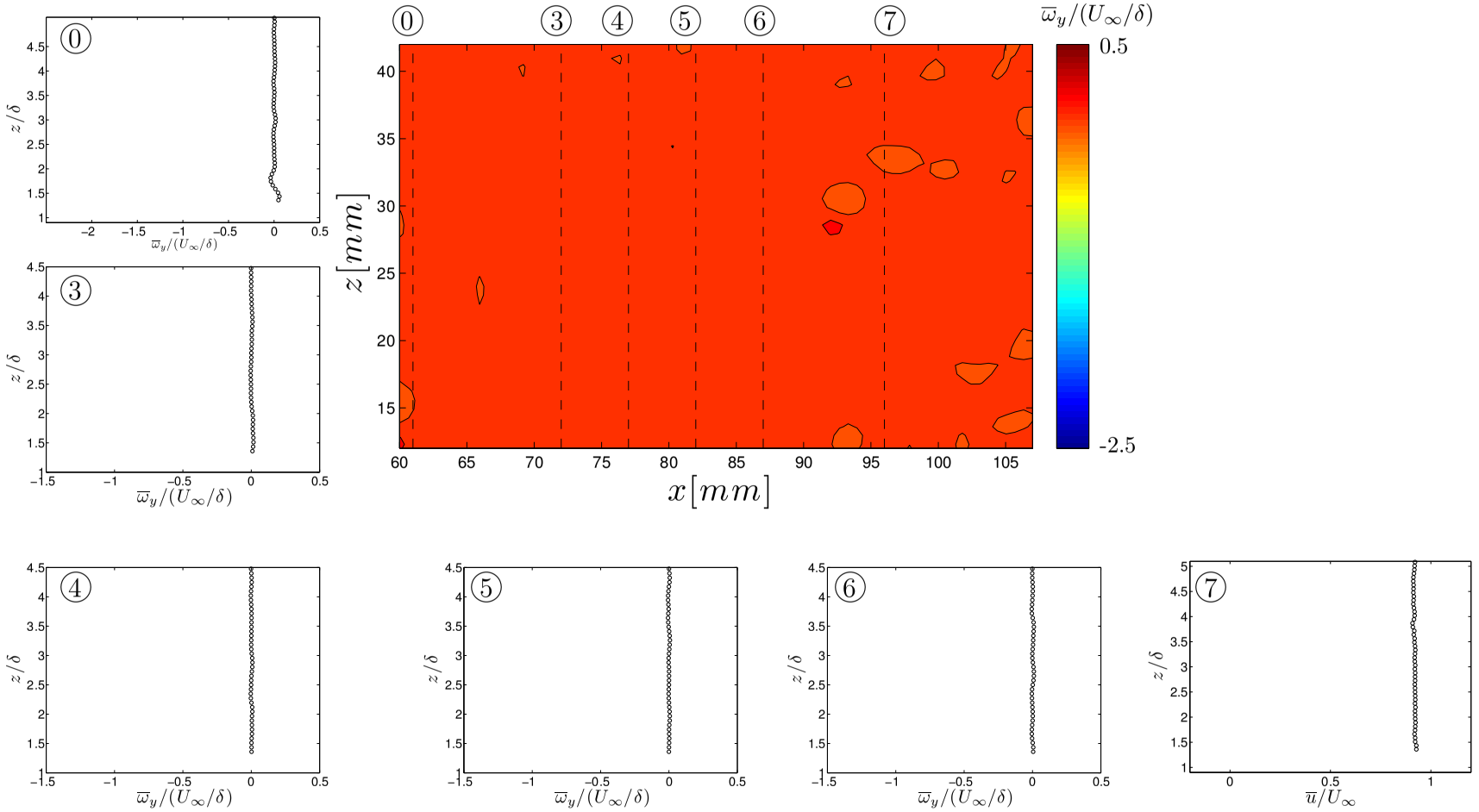

Figure C.16: Evolution of $\overline{\omega}_y/(U_\infty/\delta)$ through the y=28.5mm SBLI region for a flow deflection angle of $\theta = 6$ deg. Sampling numbers correspond to transverse plane sampling locations, location '0' indicating the region where U_∞ was calculated. At top, colors show the $\overline{\omega}_y/(U_\infty/\delta)$ field throughout each sampling plane, and also indicate their relative locations.

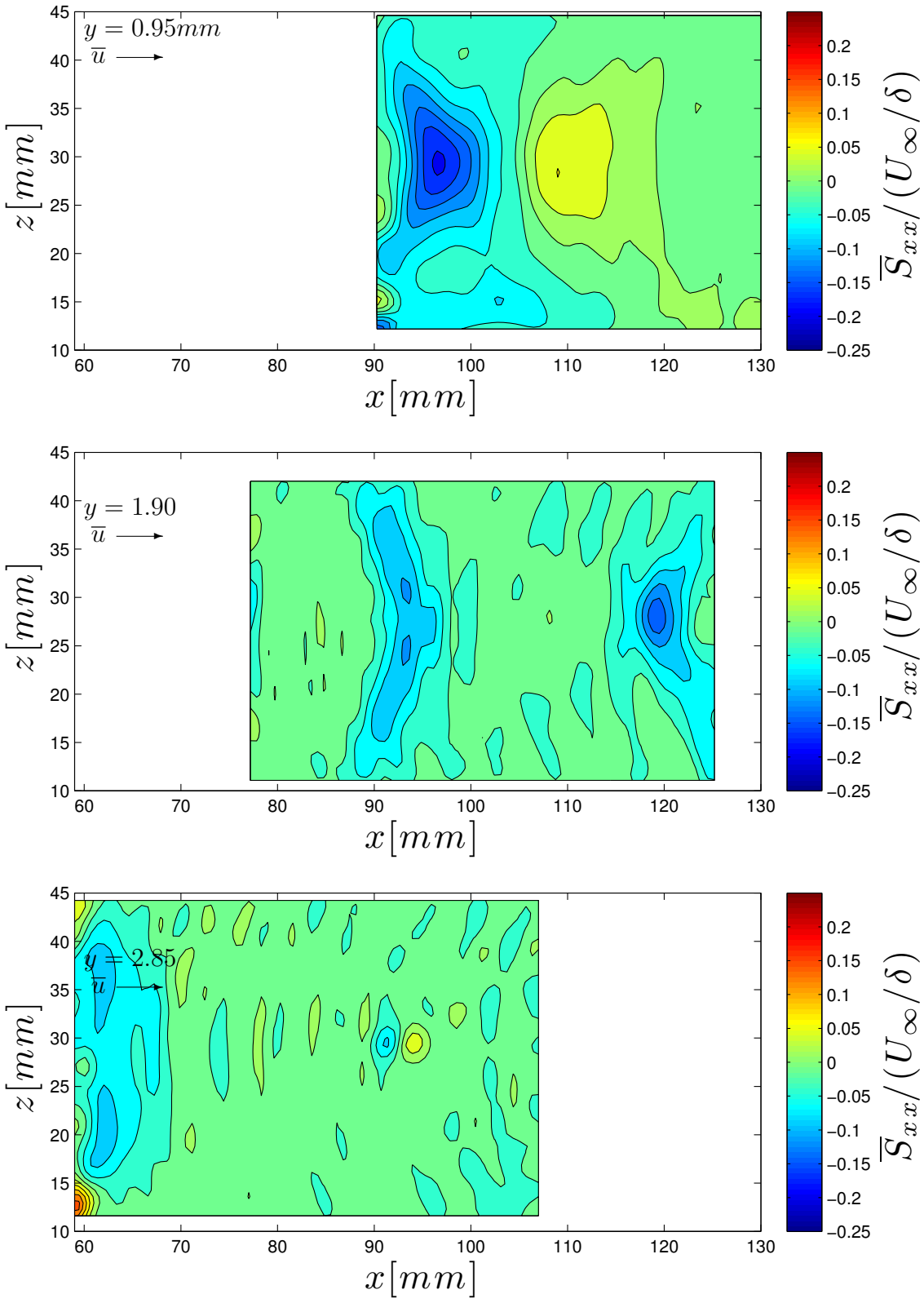

Figure C.17: Streamwise Normal Strain $\overline{S}_{xx}/(U_\infty/\delta)$ for each of the three horizontal planes oriented in the streamwise direction.

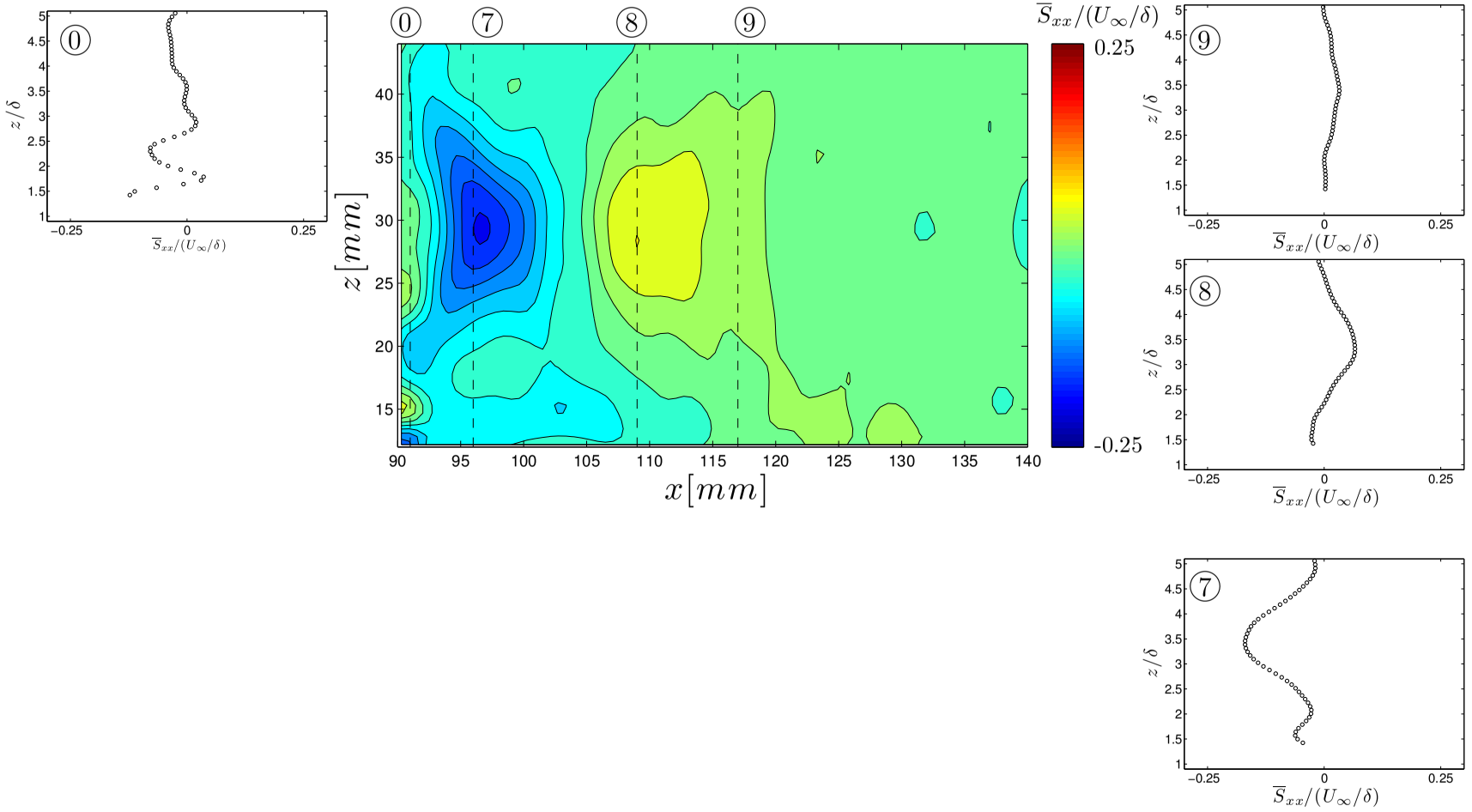

Figure C.18: Evolution of $\overline{S}_{xx}/(U_\infty/\delta)$ through the y=18mm SBLI region for a flow deflection angle of $\theta = 6$ deg. Sampling numbers correspond to transverse plane sampling locations, location '0' indicating the region where U_∞ was calculated. At top, colors show the $\overline{S}_{xx}/(U_\infty/\delta)$ field throughout each sampling plane, and also indicate their relative locations.

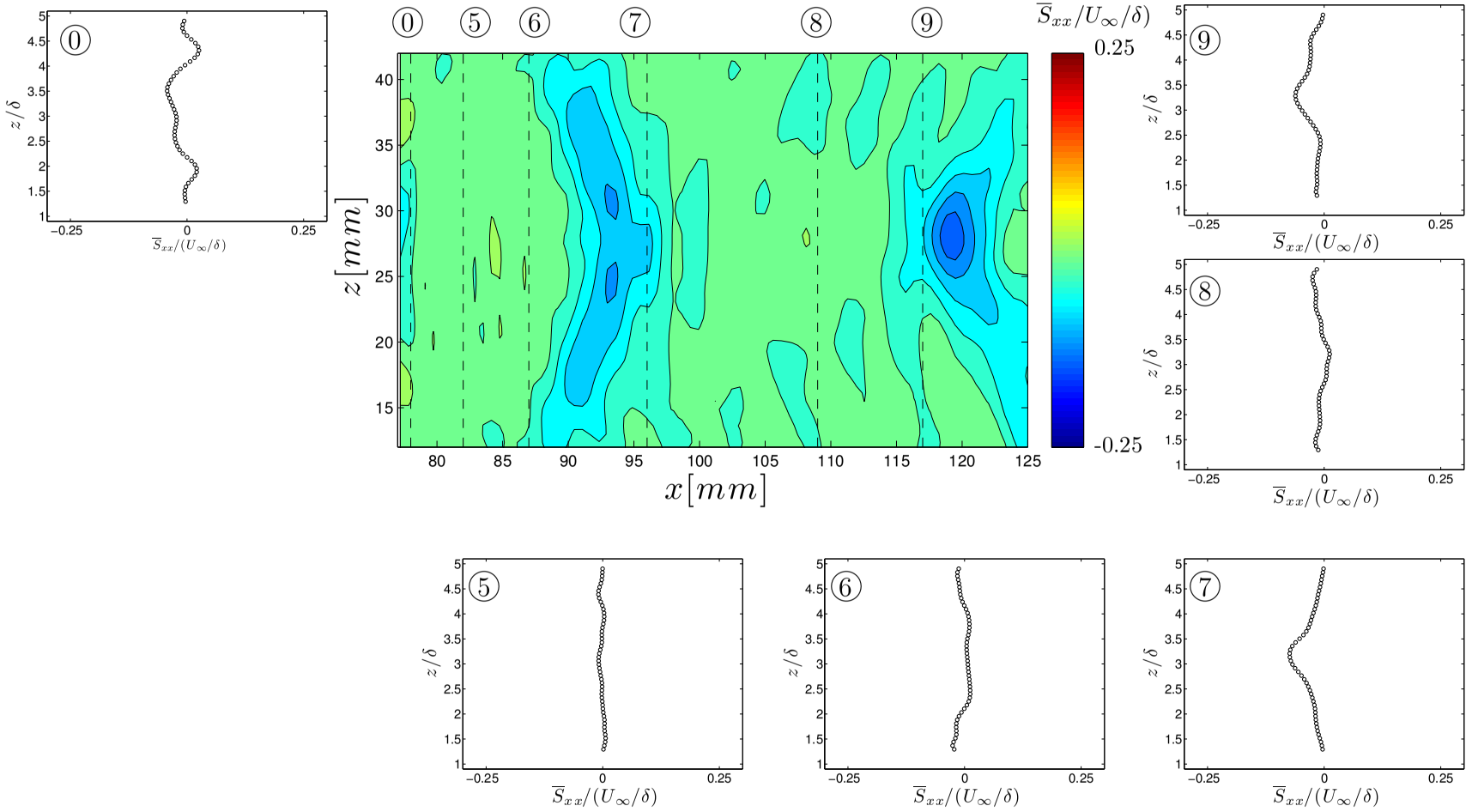

Figure C.19: Evolution of $\overline{S}_{xx}/(U_\infty/\delta)$ through the y=19mm SBLI region for a flow deflection angle of $\theta = 6$ deg. Sampling numbers correspond to transverse plane sampling locations, location '0' indicating the region where U_∞ was calculated. At top, colors show the $\overline{S}_{xx}/(U_\infty/\delta)$ field throughout each sampling plane, and also indicate their relative locations.

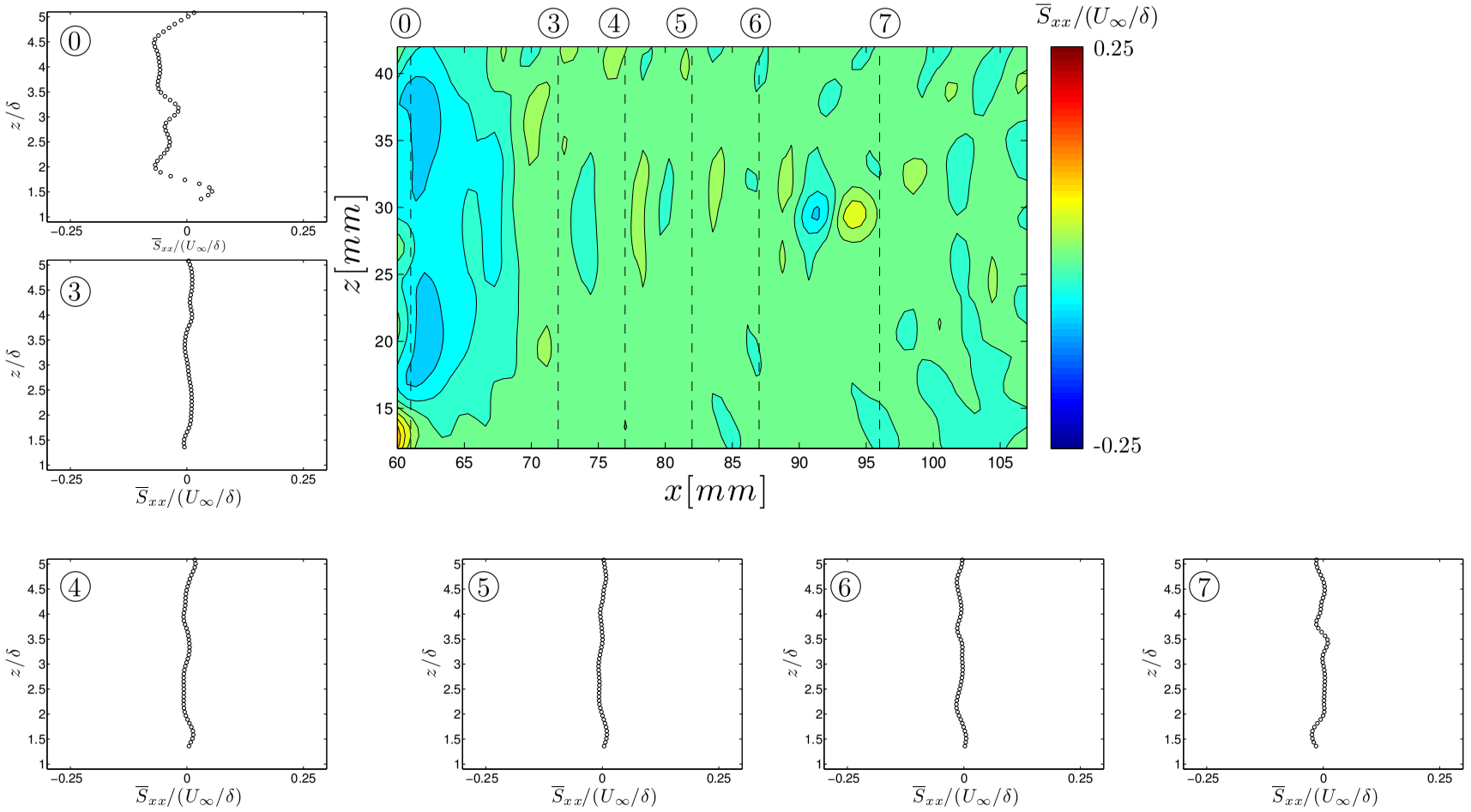

Figure C.20: Evolution of $\overline{S}_{xx}/(U_\infty/\delta)$ through the z=28.5mm SBLI region for a flow deflection angle of $\theta = 6$ deg. Sampling numbers correspond to transverse plane sampling locations, location '0' indicating the region where U_∞ was calculated. At top, colors show the $\overline{S}_{xx}/(U_\infty/\delta)$ field throughout each sampling plane, and also indicate their relative locations.

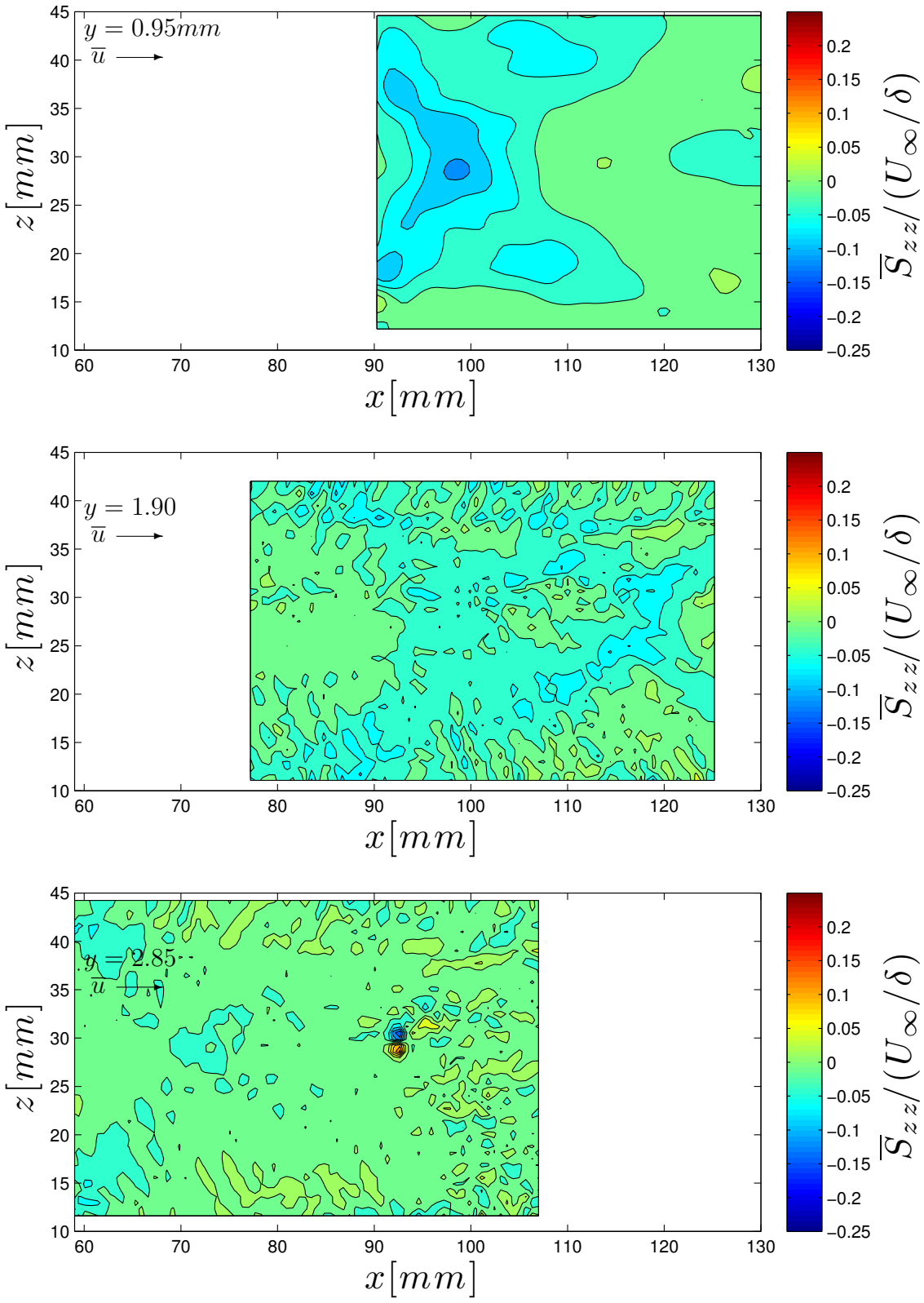

Figure C.21: Streamwise Normal Strain $\overline{S}_{zz}/(U_\infty/\delta)$ for each of the three horizontal planes oriented in the streamwise direction.

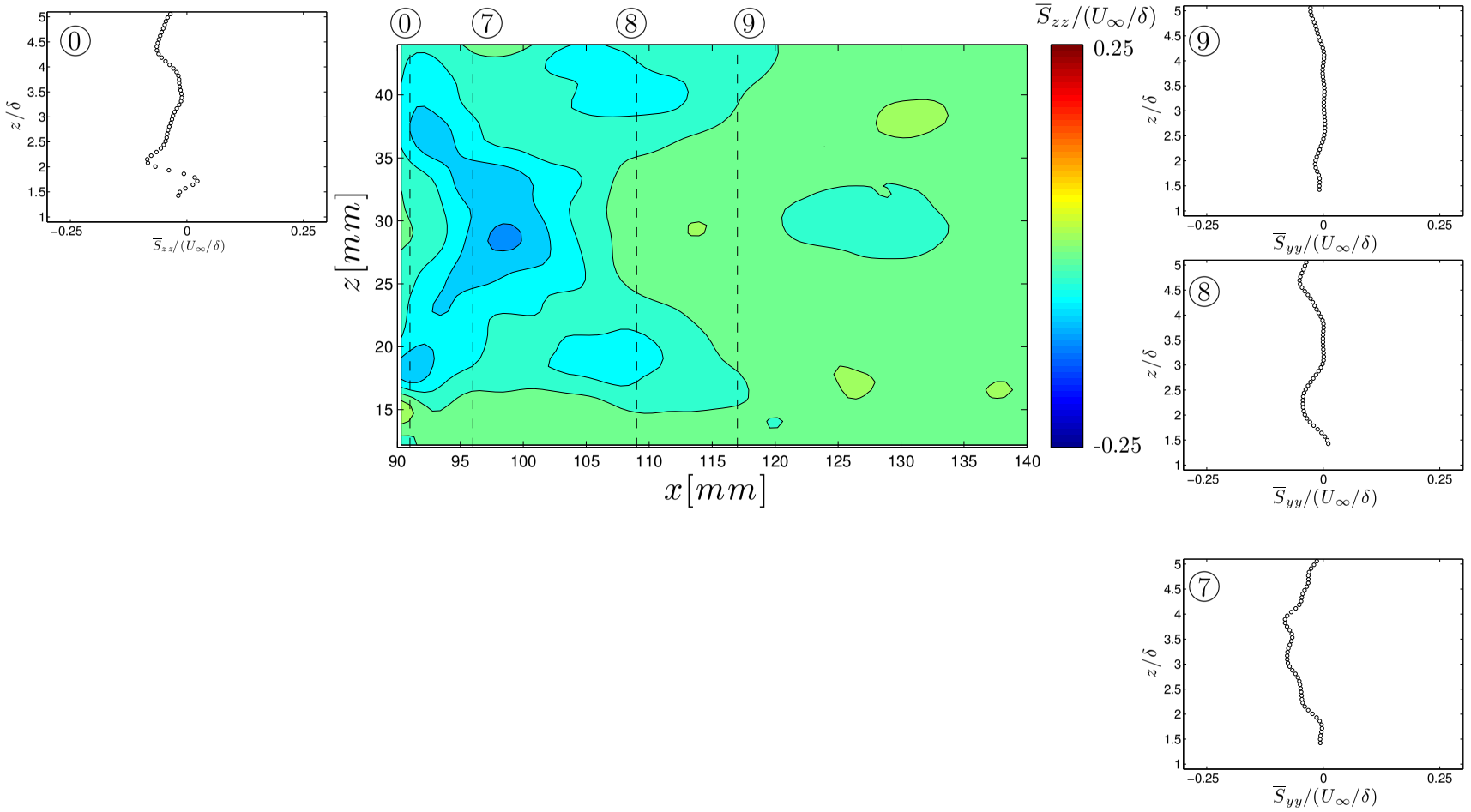

Figure C.22: Evolution of $\overline{S}_{zz}/(U_\infty/\delta)$ through the y=18mm SBLI region for a flow deflection angle of $\theta = 6$ deg. Sampling numbers correspond to transverse plane sampling locations, location '0' indicating the region where U_∞ was calculated. At top, colors show the $\overline{S}_{zz}/(U_\infty/\delta)$ field throughout each sampling plane, and also indicate their relative locations.

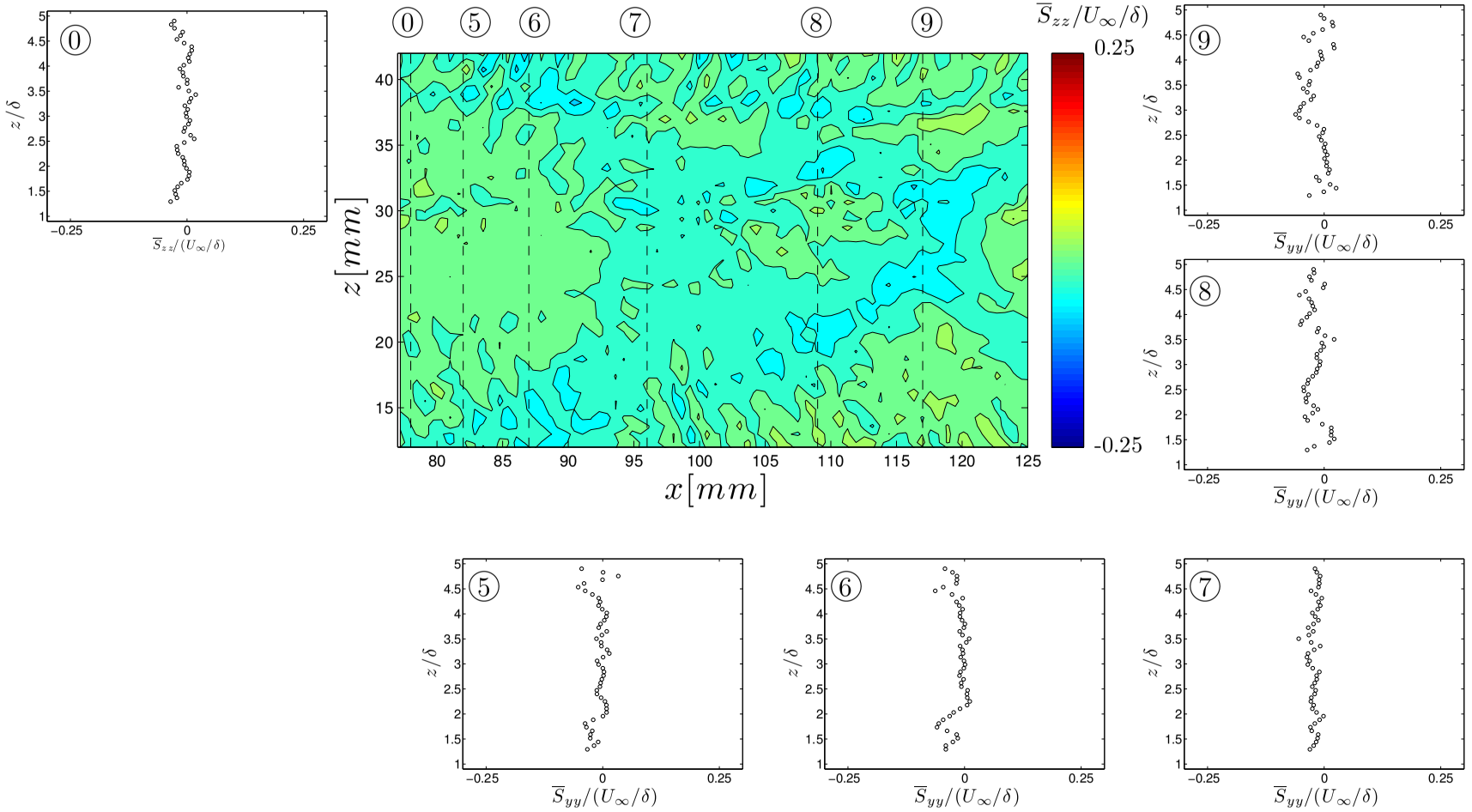

Figure C.23: Evolution of $\overline{S}_{zz}/(U_\infty/\delta)$ through the y=19mm SBLI region for a flow deflection angle of $\theta = 6$ deg. Sampling numbers correspond to transverse plane sampling locations, location '0' indicating the region where U_∞ was calculated. At top, colors show the $\overline{S}_{zz}/(U_\infty/\delta)$ field throughout each sampling plane, and also indicate their relative locations.

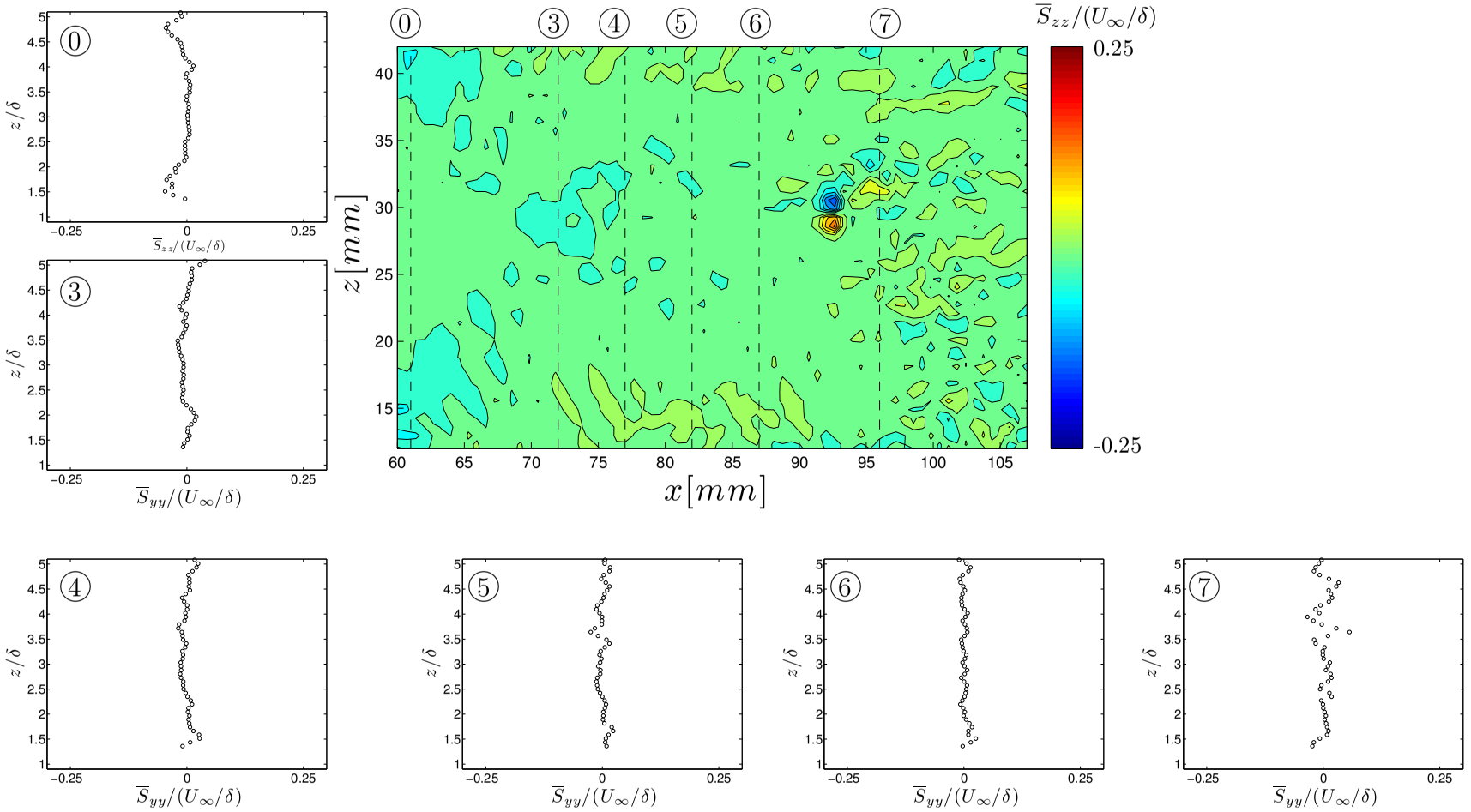

Figure C.24: Evolution of $\overline{S}_{zz}/(U_\infty/\delta)$ through the z=18mm SBLI region for a flow deflection angle of $\theta = 6$ deg. Sampling numbers correspond to transverse plane sampling locations, location '0' indicating the region where U_∞ was calculated. At top, colors show the $\overline{S}_{zz}/(U_\infty/\delta)$ field throughout each sampling plane, and also indicate their relative locations.

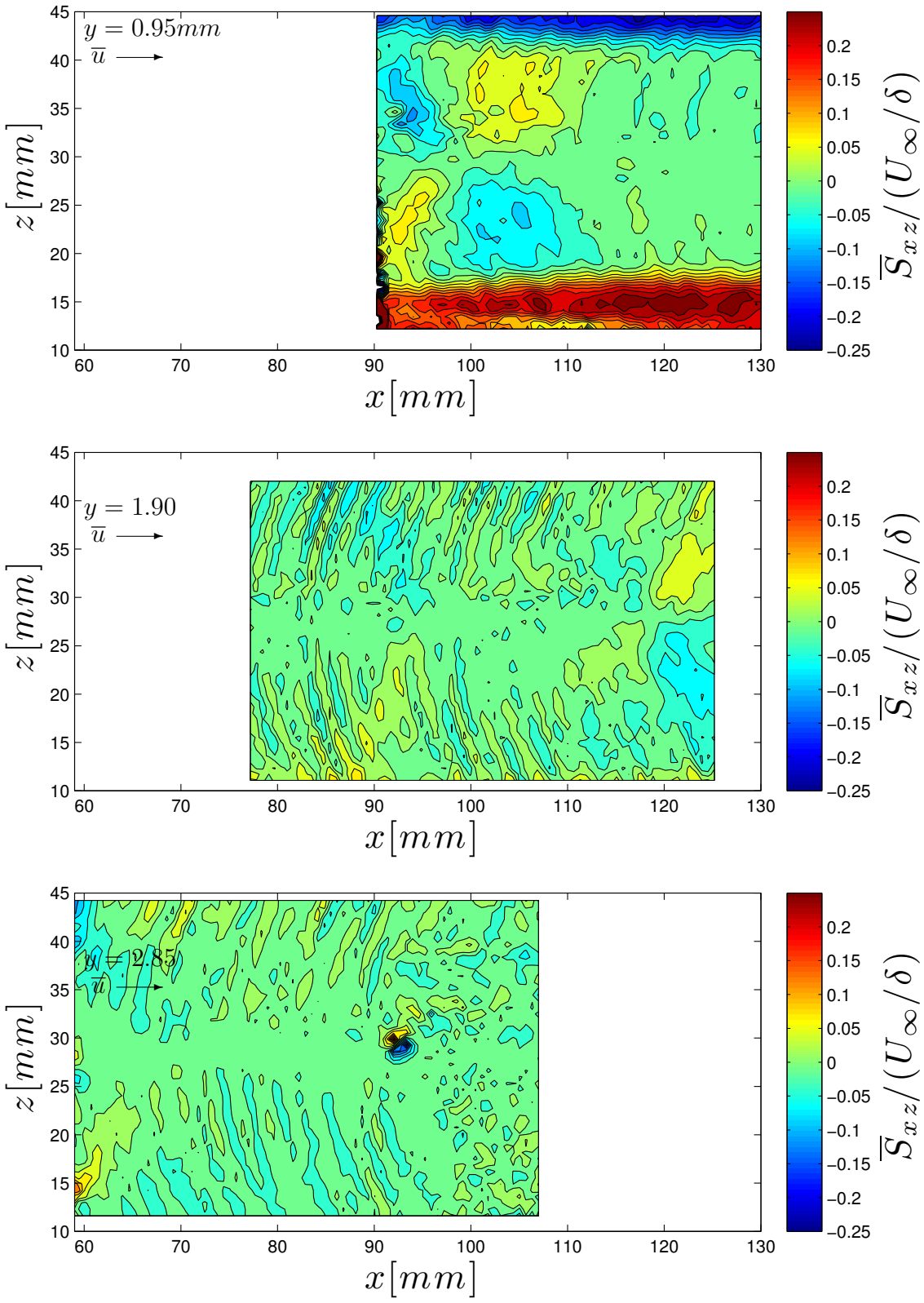

Figure C.25: Streamwise Normal Strain $\overline{S}_{xz}/(U_\infty/\delta)$ for each of the three horizontal planes oriented in the streamwise direction.

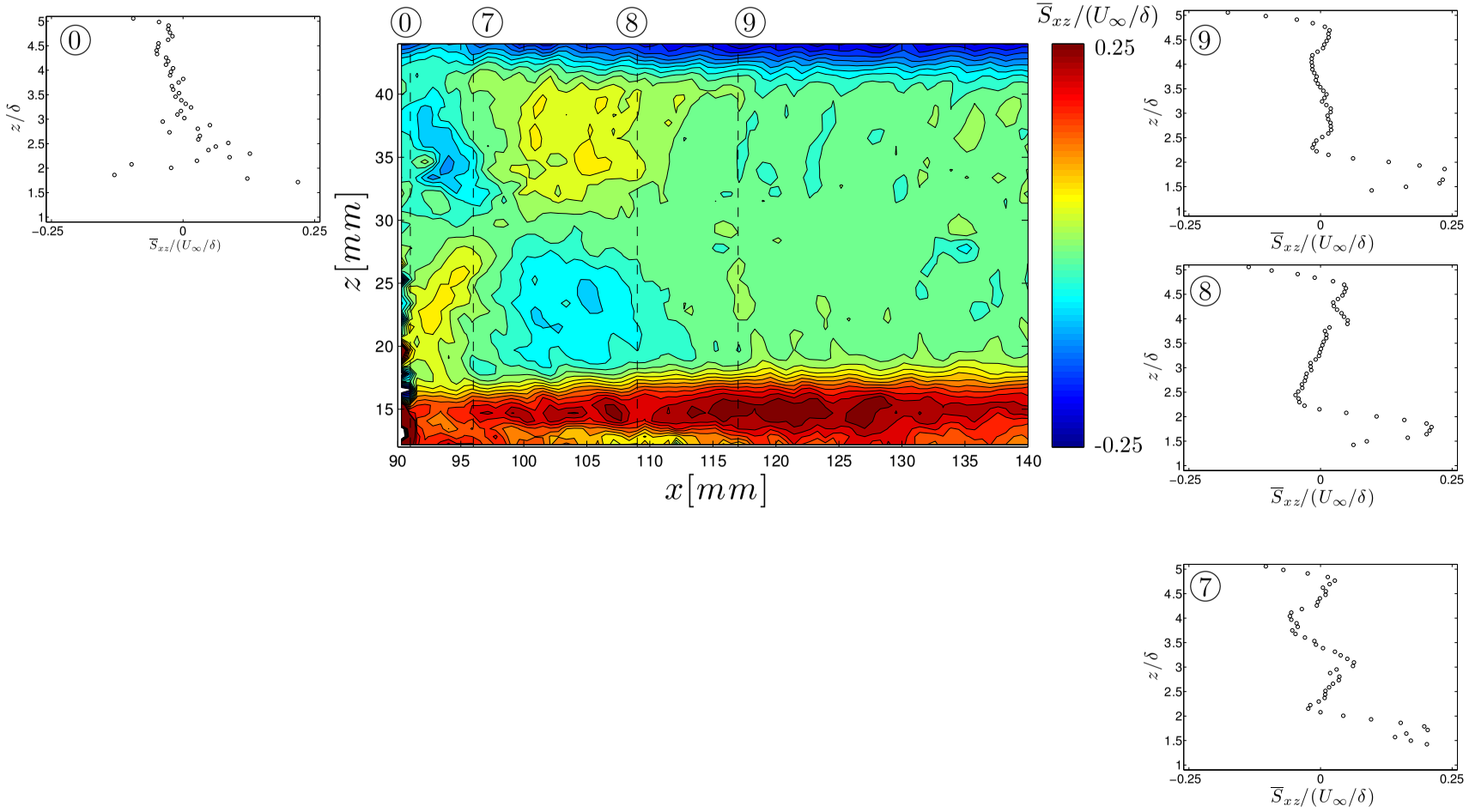

Figure C.26: Evolution of $\overline{S}_{xz}/(U_\infty/\delta)$ through the y=18mm SBLI region for a flow deflection angle of $\theta = 6$ deg. Sampling numbers correspond to transverse plane sampling locations, location '0' indicating the region where U_∞ was calculated. At top, colors show the $\overline{S}_{xz}/(U_\infty/\delta)$ field throughout each sampling plane, and also indicate their relative locations.

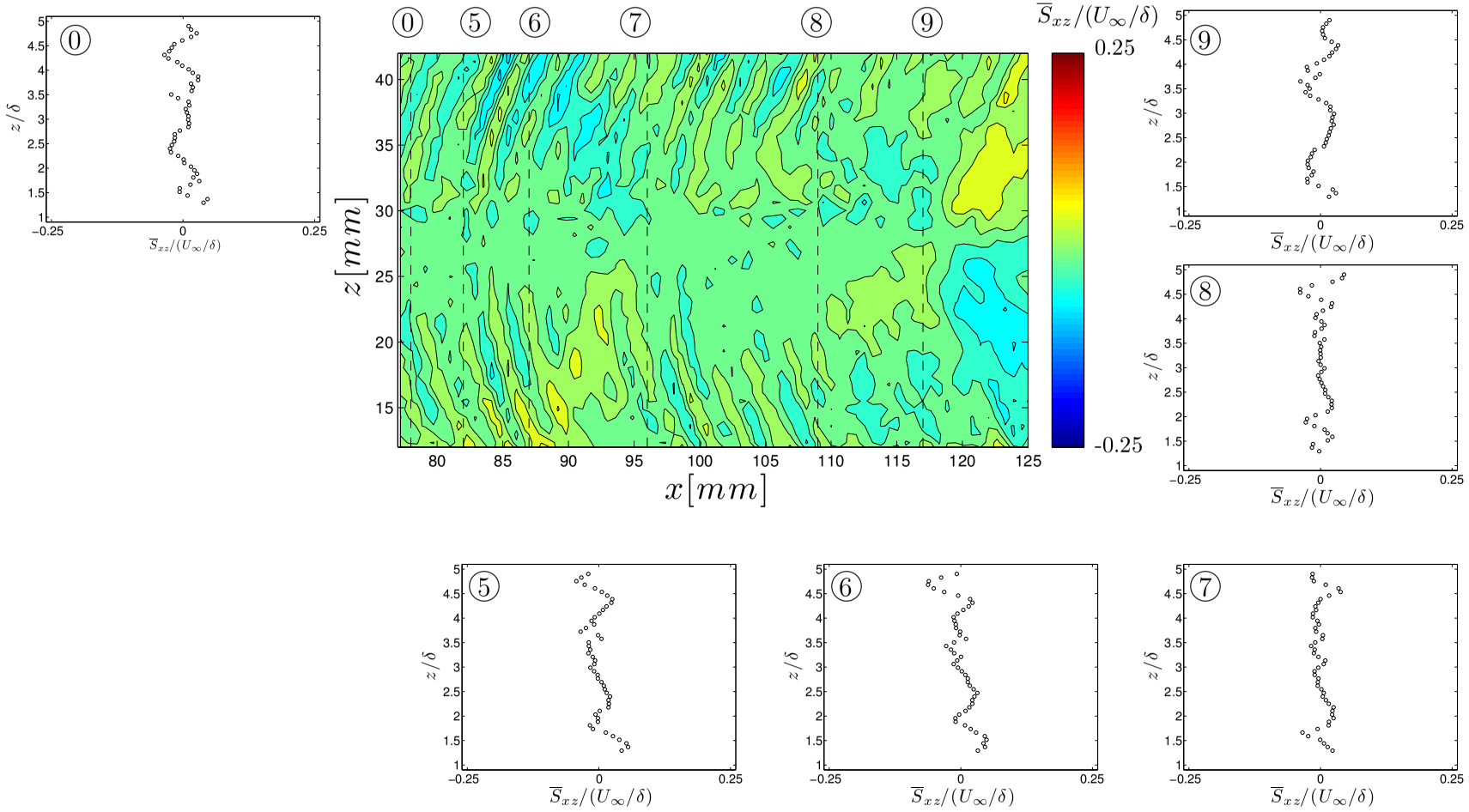

Figure C.27: Evolution of $\overline{S}_{xz}/(U_\infty/\delta)$ through the y=19mm SBLI region for a flow deflection angle of $\theta = 6$ deg. Sampling numbers correspond to transverse plane sampling locations, location '0' indicating the region where U_∞ was calculated. At top, colors show the $\overline{S}_{xz}/(U_\infty/\delta)$ field throughout each sampling plane, and also indicate their relative locations.

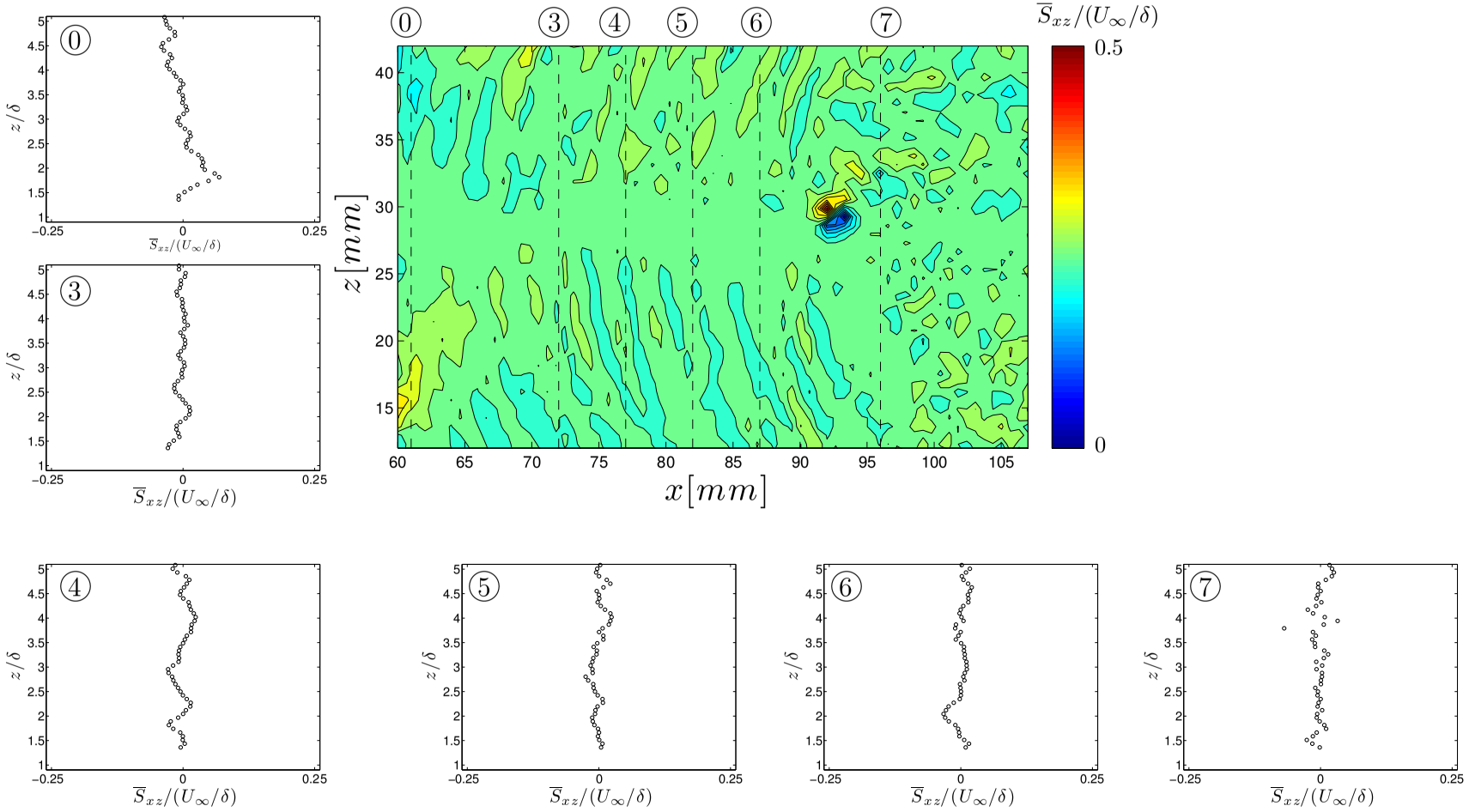

Figure C.28: Evolution of $\overline{S}_{xz}/(U_\infty/\delta)$ through the z=18mm SBLI region for a flow deflection angle of $\theta = 6$ deg. Sampling numbers correspond to transverse plane sampling locations, location '0' indicating the region where U_∞ was calculated. At top, colors show the $\overline{S}_{xz}/(U_\infty/\delta)$ field throughout each sampling plane, and also indicate their relative locations.

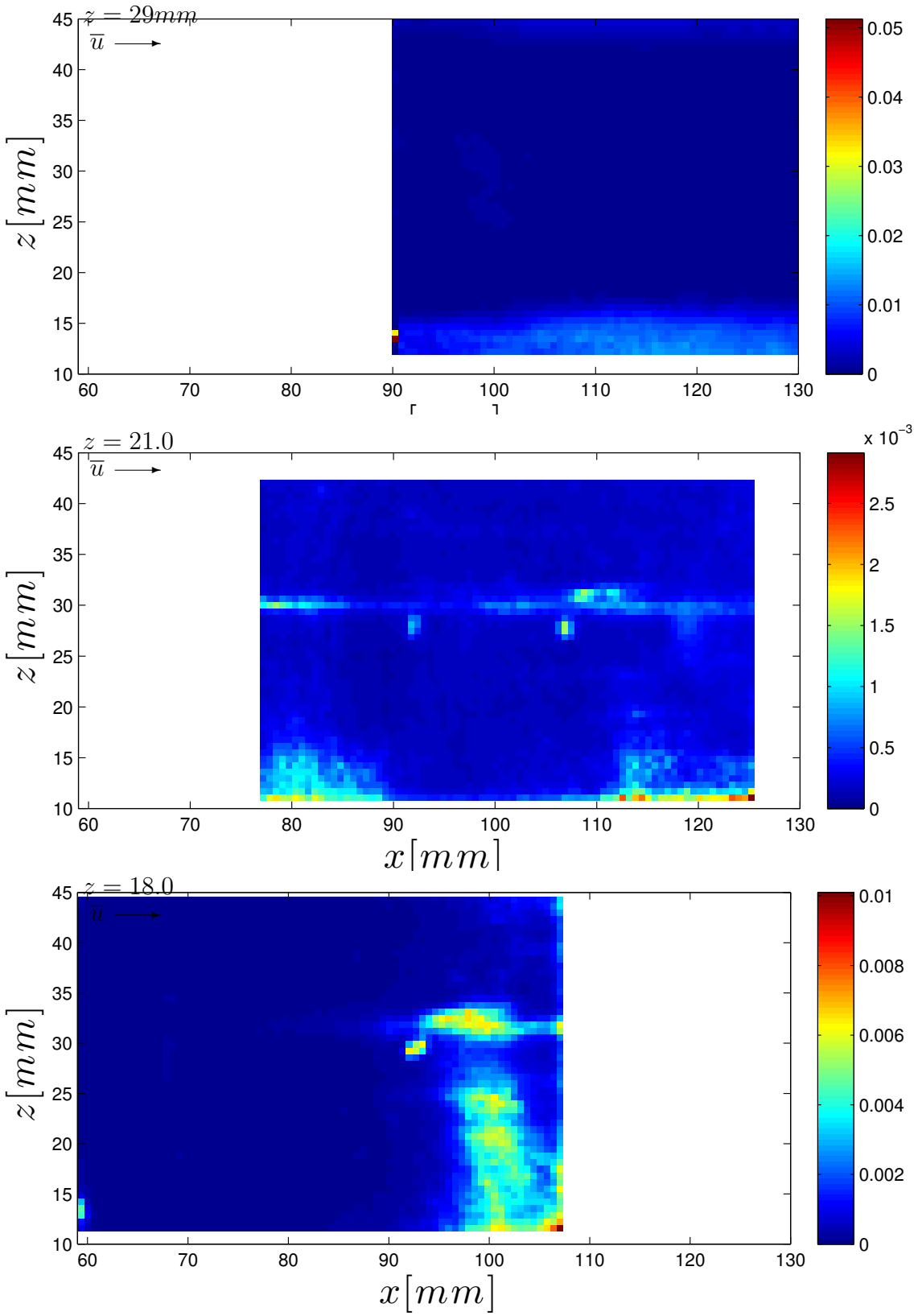

Figure C.29: Visualizations of the normalized Reynold's stress component $\overline{u'^2}$ for each of the three horizontal planes oriented in the streamwise direction.

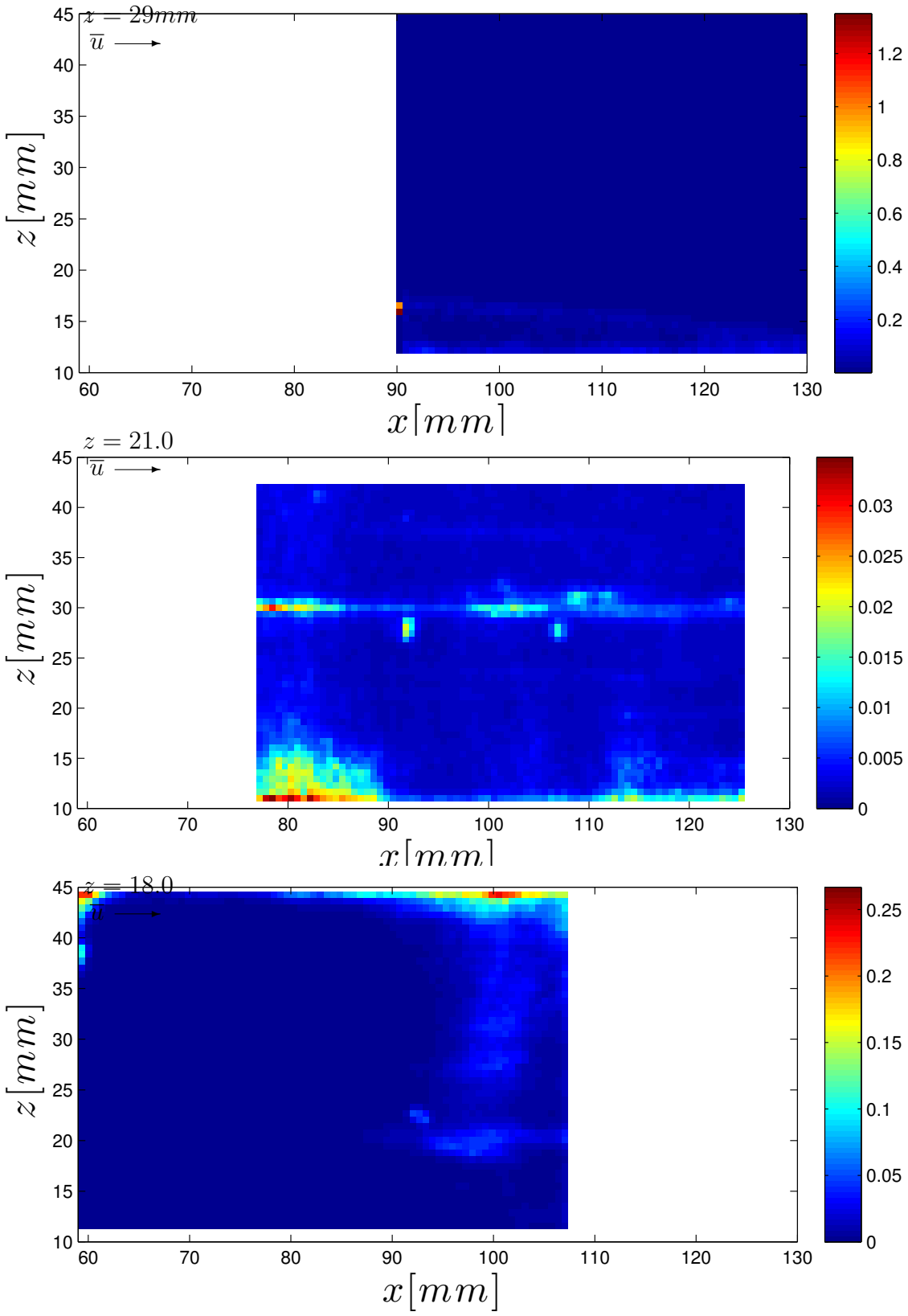

Figure C.30: Visualizations of the normalized Reynold's stress component $\overline{v'^2}$ for each of the three horizontal planes oriented in the streamwise direction.

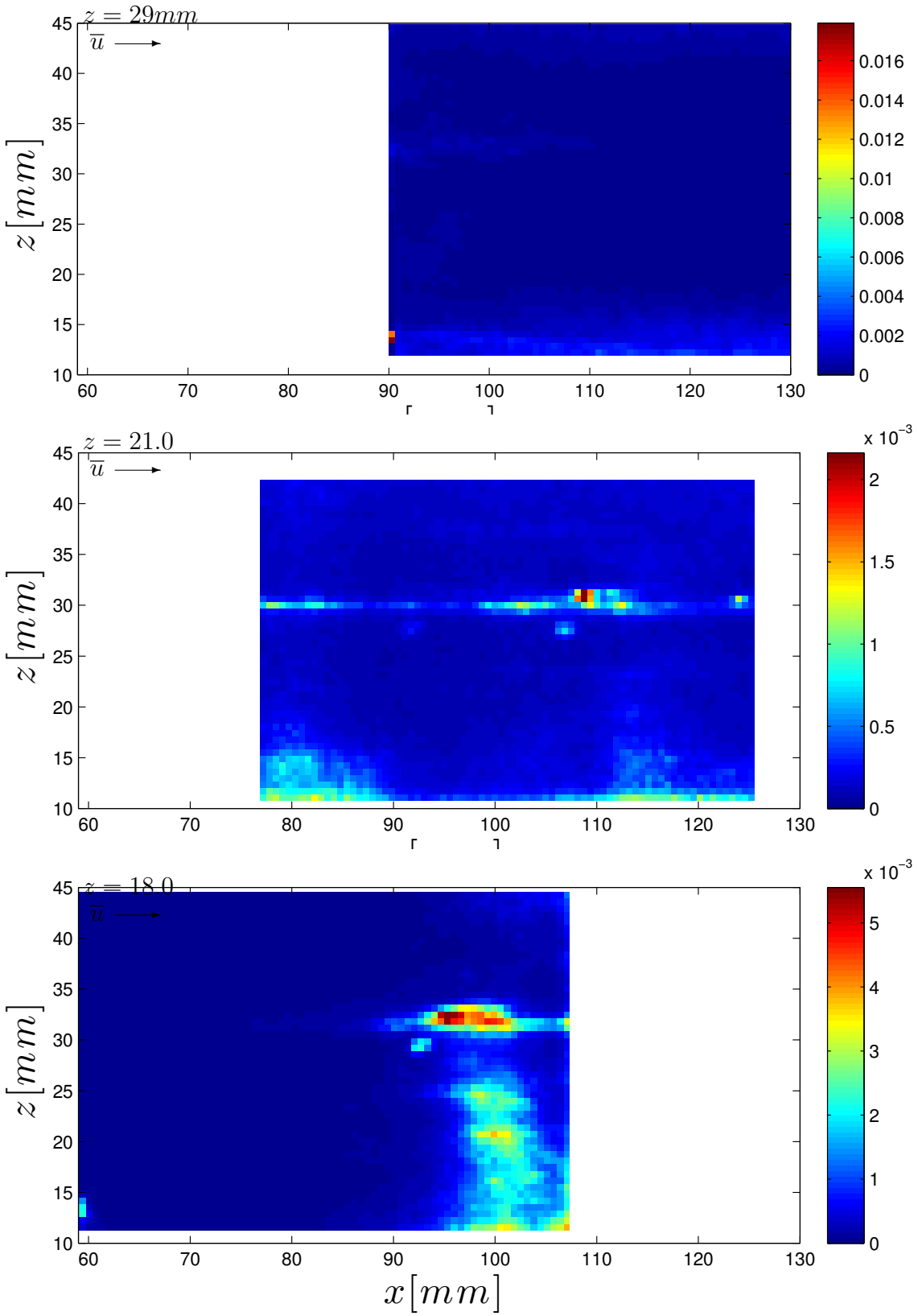

Figure C.31: Visualizations of the normalized Reynold's stress component $\overline{w'^2}$ for each of the three horizontal planes oriented in the streamwise direction.

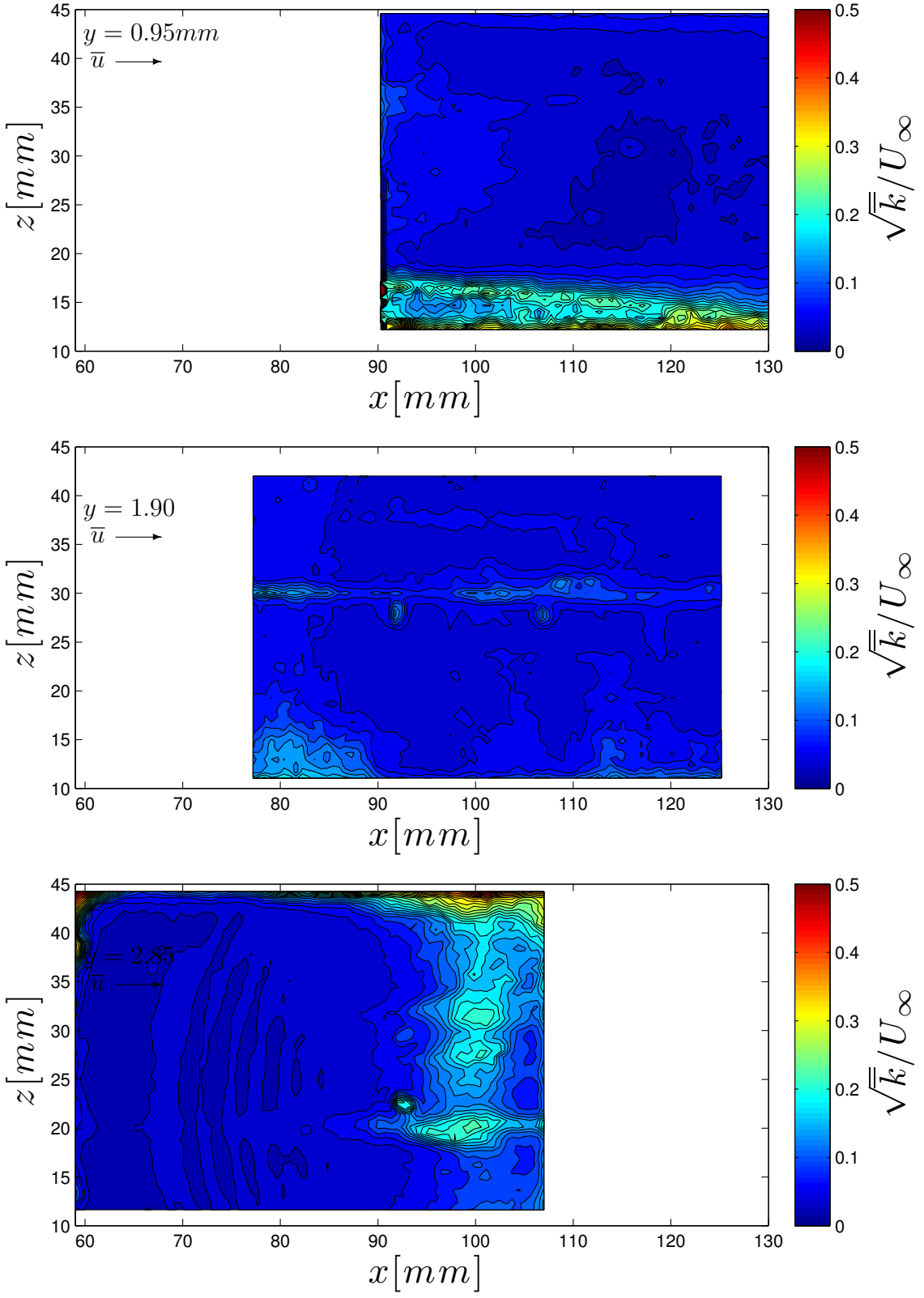

Figure C.32: Turbulent Kinetic Energy $\sqrt{\overline{k}}/U_\infty$ for each of the three horizontal planes oriented in the streamwise direction.

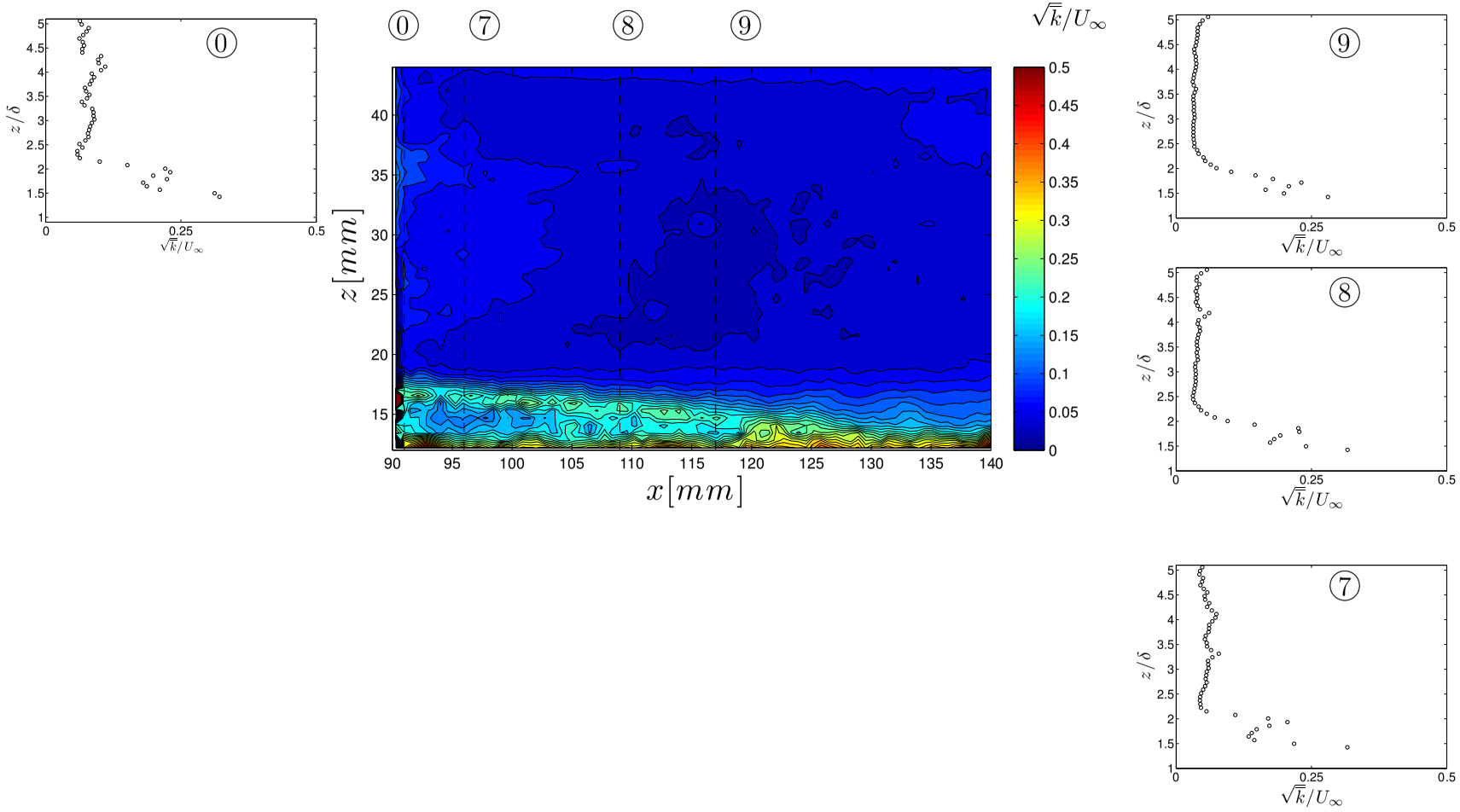

Figure C.33: Evolution of $\sqrt{\overline{k}}/U_\infty$ through the y=9.5mm SBLI region for a flow deflection angle of $\theta = 6$ deg. Sampling numbers correspond to transverse plane sampling locations, location '0' indicating the region where U_∞ was calculated. At top, colors show the $\sqrt{\overline{k}}/U_\infty$ field throughout each sampling plane, and also indicate their relative locations.

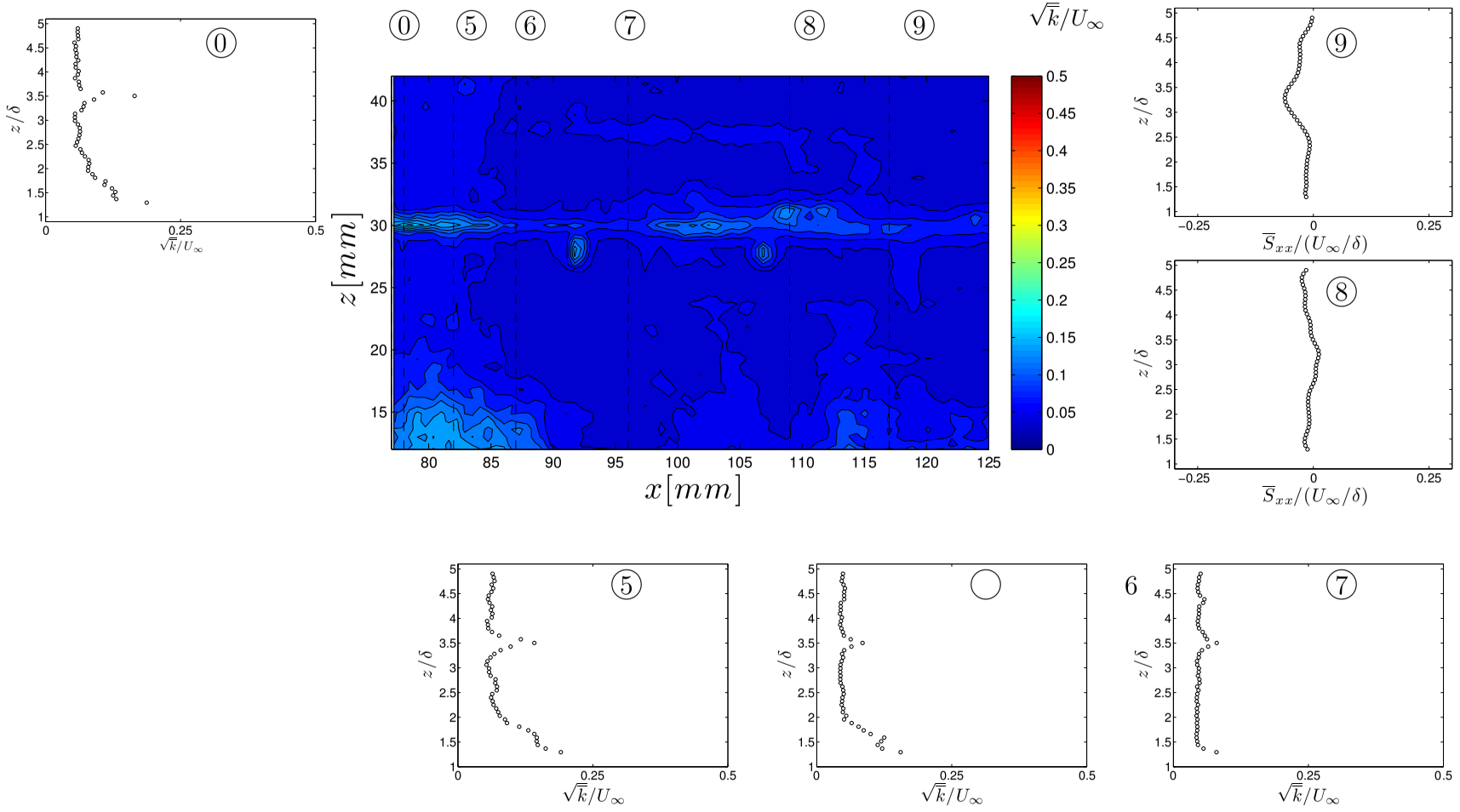

Figure C.34: Evolution of $\sqrt{\overline{k}}/U_\infty$through the y=18mm SBLI region for a flow deflection angle of $\theta = 6$ deg. Sampling numbers correspond to transverse plane sampling locations, location '0' indicating the region where U_∞ was calculated. At top, colors show the $\sqrt{\overline{k}}/U_\infty$ field throughout each sampling plane, and also indicate their relative locations.

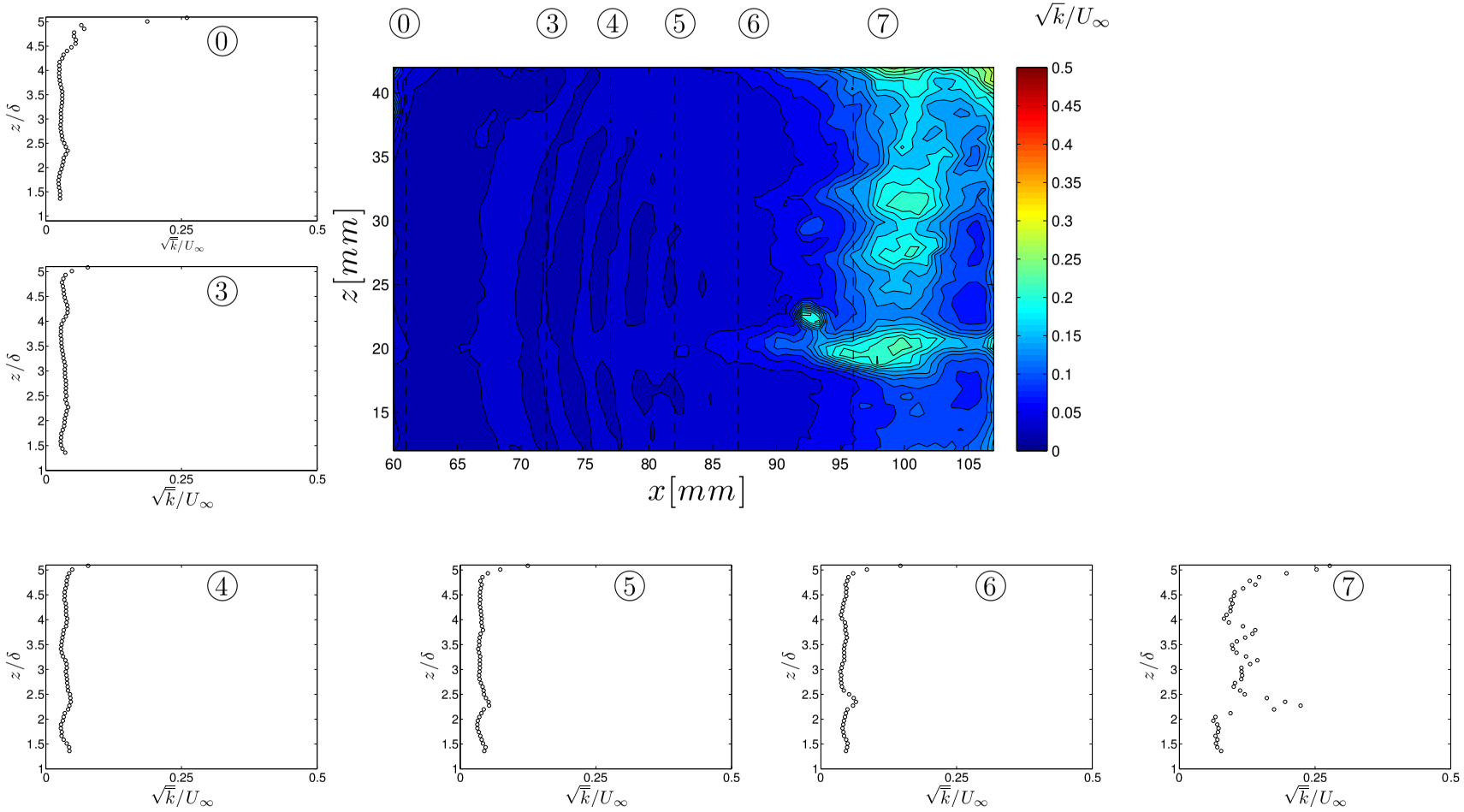

Figure C.35: Evolution of $\sqrt{k}/U_\infty$ through the y=28.5mm SBLI region for a flow deflection angle of $\theta = 6$ deg. Sampling numbers correspond to transverse plane sampling locations, location '0' indicating the region where U_∞ was calculated. At top, colors show the $\sqrt{k}/U_\infty$ field throughout each sampling plane, and also indicate their relative locations.

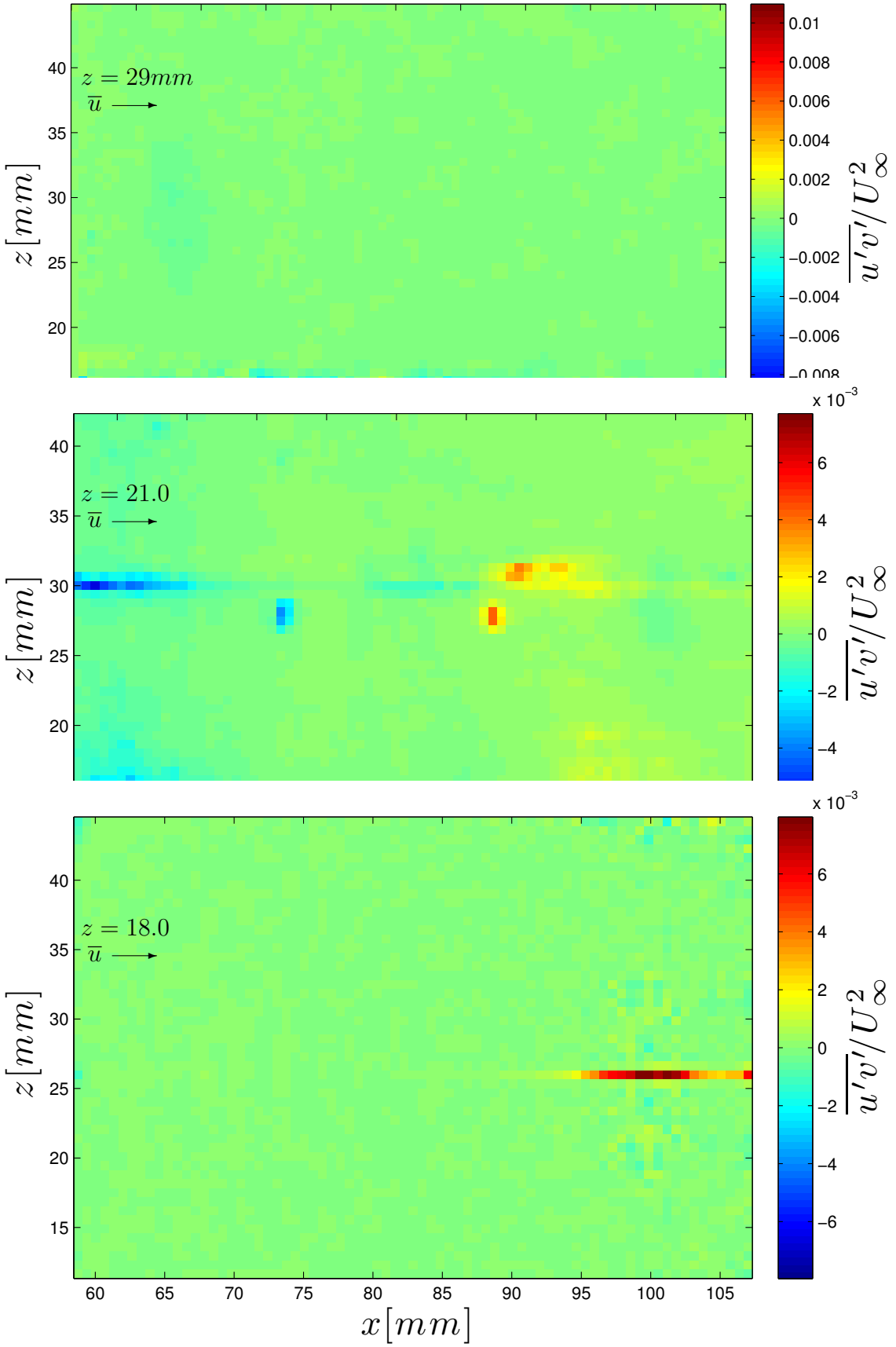

Figure C.36: Visualizations of the normalized Reynold's stress component $\overline{u'v'}$ for each of the three horizontal planes oriented in the streamwise direction.

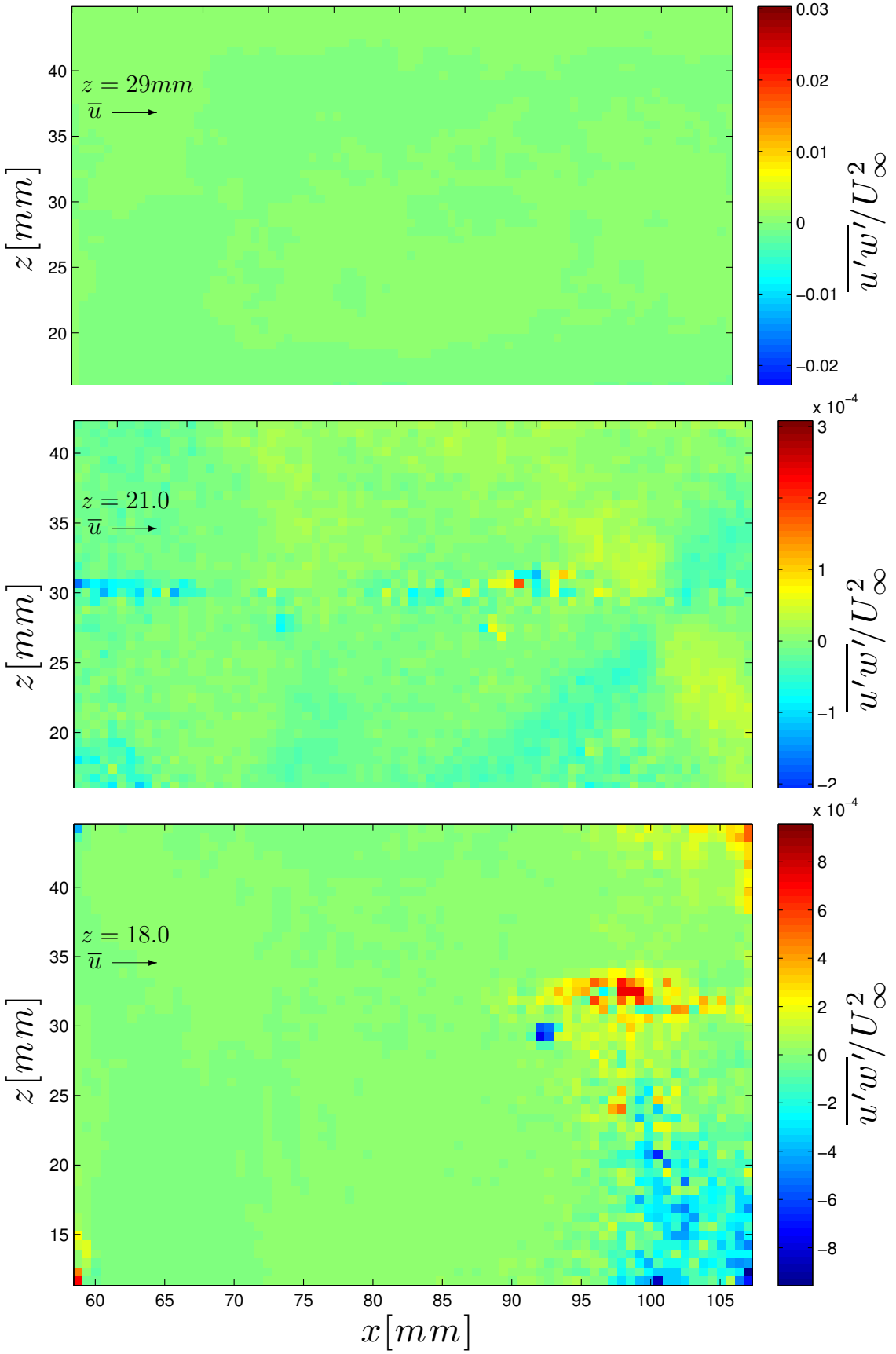

Figure C.37: Visualizations of the normalized Reynold's stress component $\overline{u'w'}$ for each of the three horizontal planes oriented in the streamwise direction.

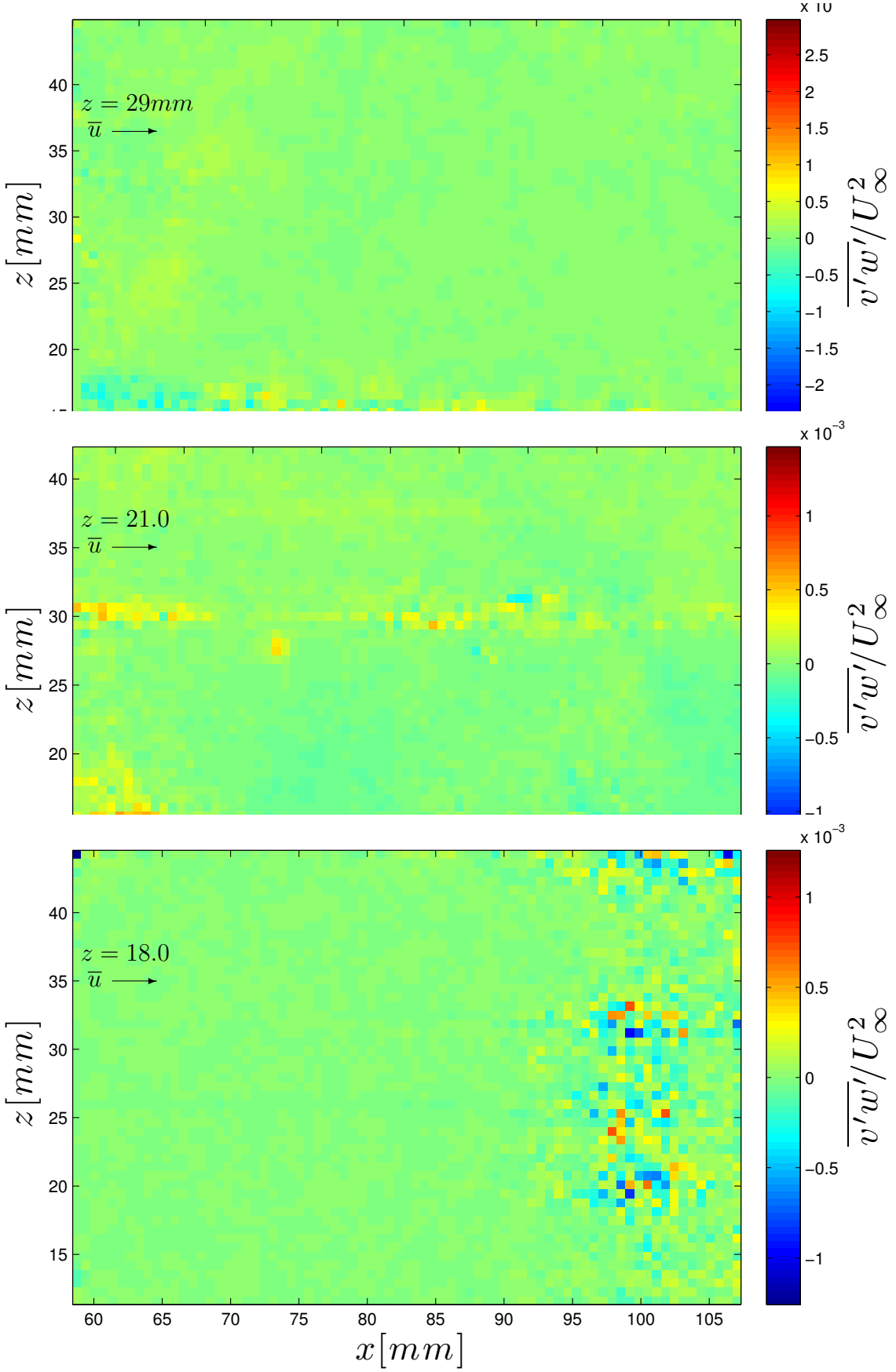

Figure C.38: Visualizations of the normalized Reynold's stress component $\overline{v'w'}$ for each of the three horizontal planes oriented in the streamwise direction.

APPENDIX D

Spanwise Vertical Data

This section presents data from the spanwise vertical planes which were not presented in the main body of the thesis. The data is presented in a consistent format first in a perspective view of all three planes oriented along a consistent axis, followed by individual profiles from each plane. Table D.1 presents the order of the quantities considered.

U Velocity	u_x
V Velocity	u_y
W Velocity	u_z
Streamwise Vorticity	ω_x
Z Normal Strain	S_{zz}
Y Normal Strain	S_{yy}
Z-Y Shear Strain	S_{zy}
X Reynolds Stress	u'^2
Y Reynolds Stress	v'^2
Z Reynolds Stress	w'^2
Turbulence Kinetic Energy	$\sqrt{\overline{k}}$
XY Reynolds Stress	$u\prime v\prime$
XZ Reynolds Stress	$u\prime w\prime$
YZ Reynolds Stress	$v\prime w\prime$

Table D.1: Presented Transverse PIV velocity data and derived quantities.

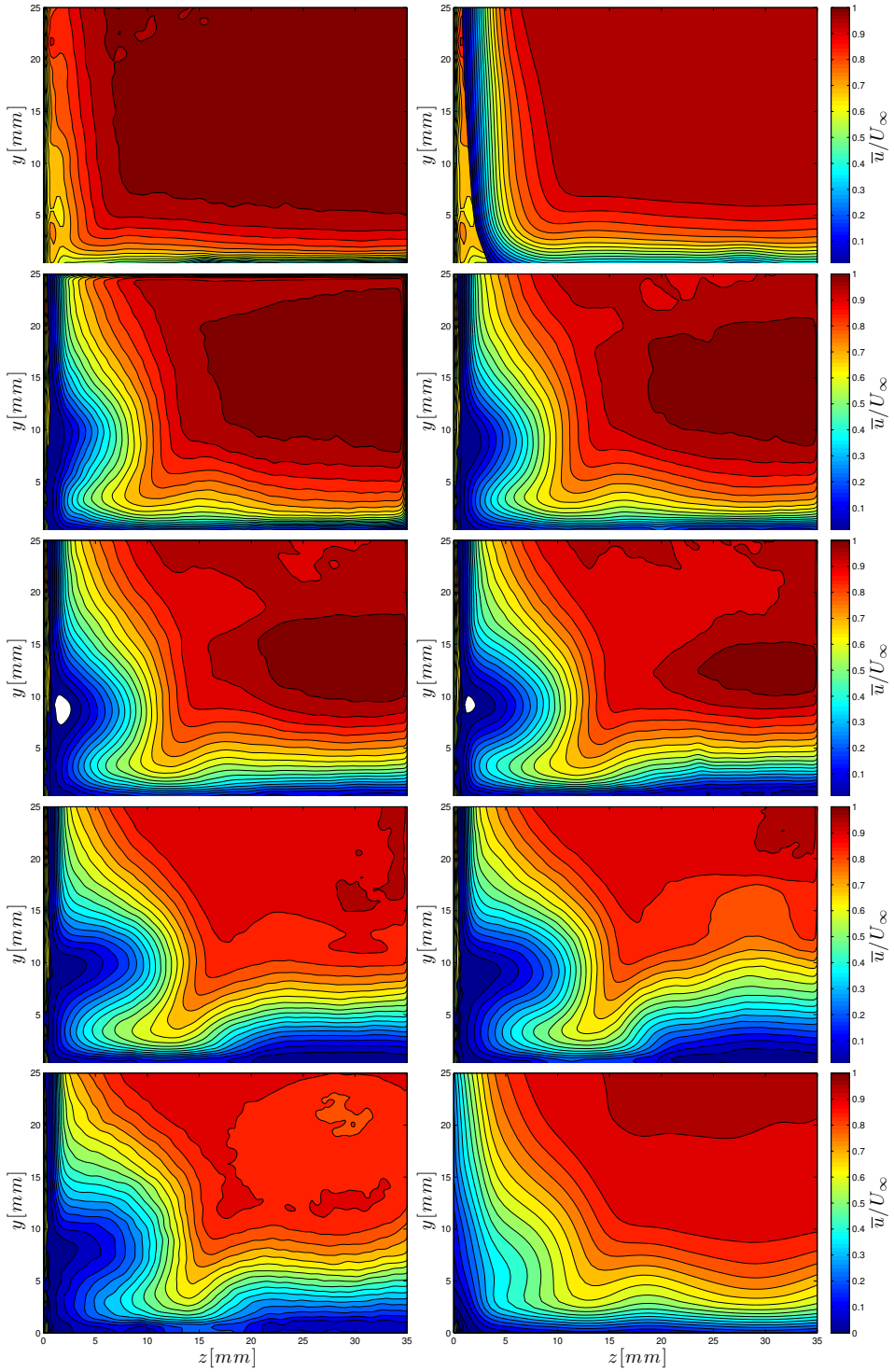

Figure D.1: Evolution of $\overline{u}/U_\infty$ through the SBLI - corner region for a flow deflection angle of $\theta = 6$–deg.

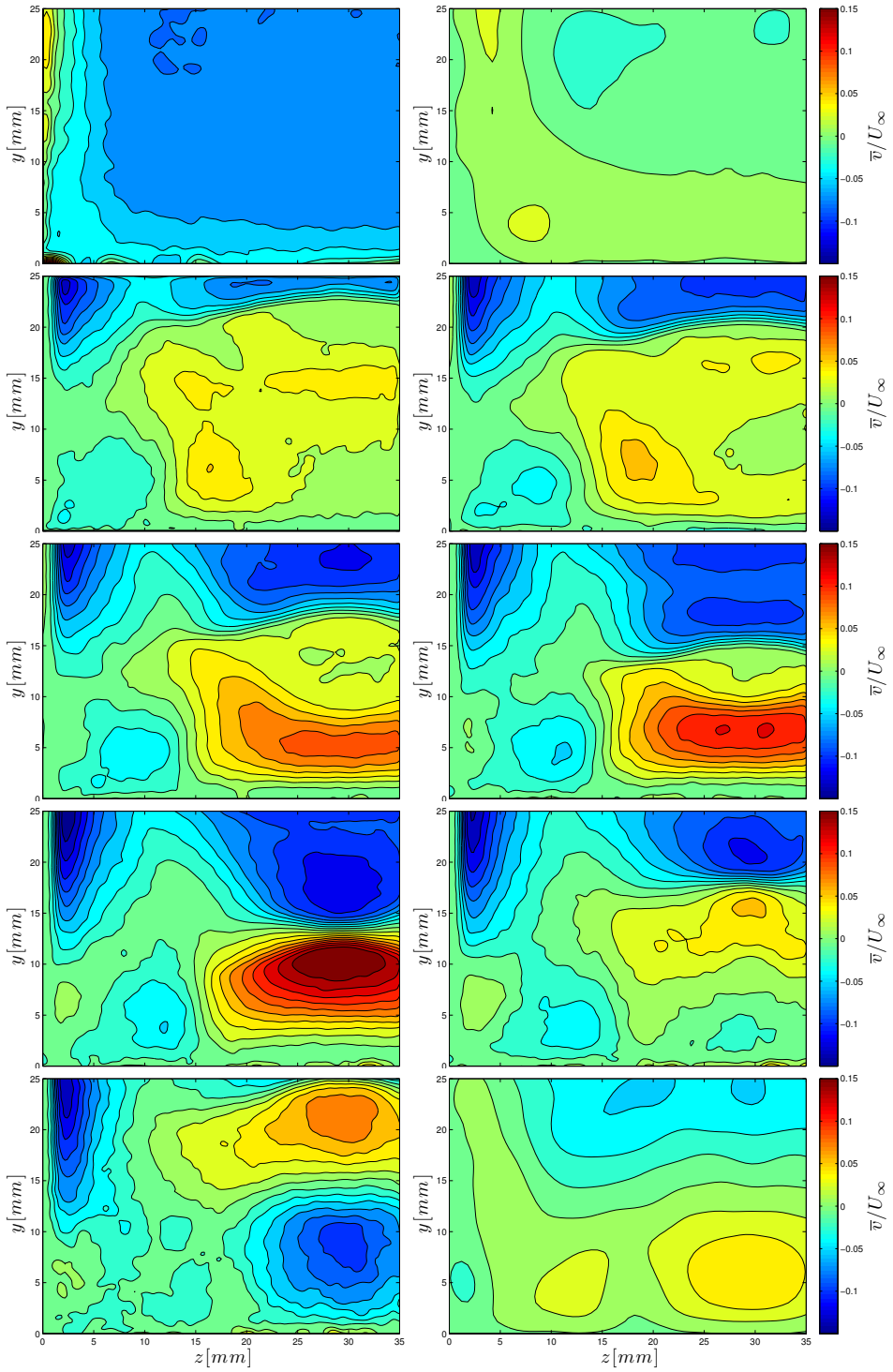

Figure D.2: Evolution of $\overline{v}/U_\infty$ through the SBLI - corner region for a flow deflection angle of $\theta = 6$–deg.

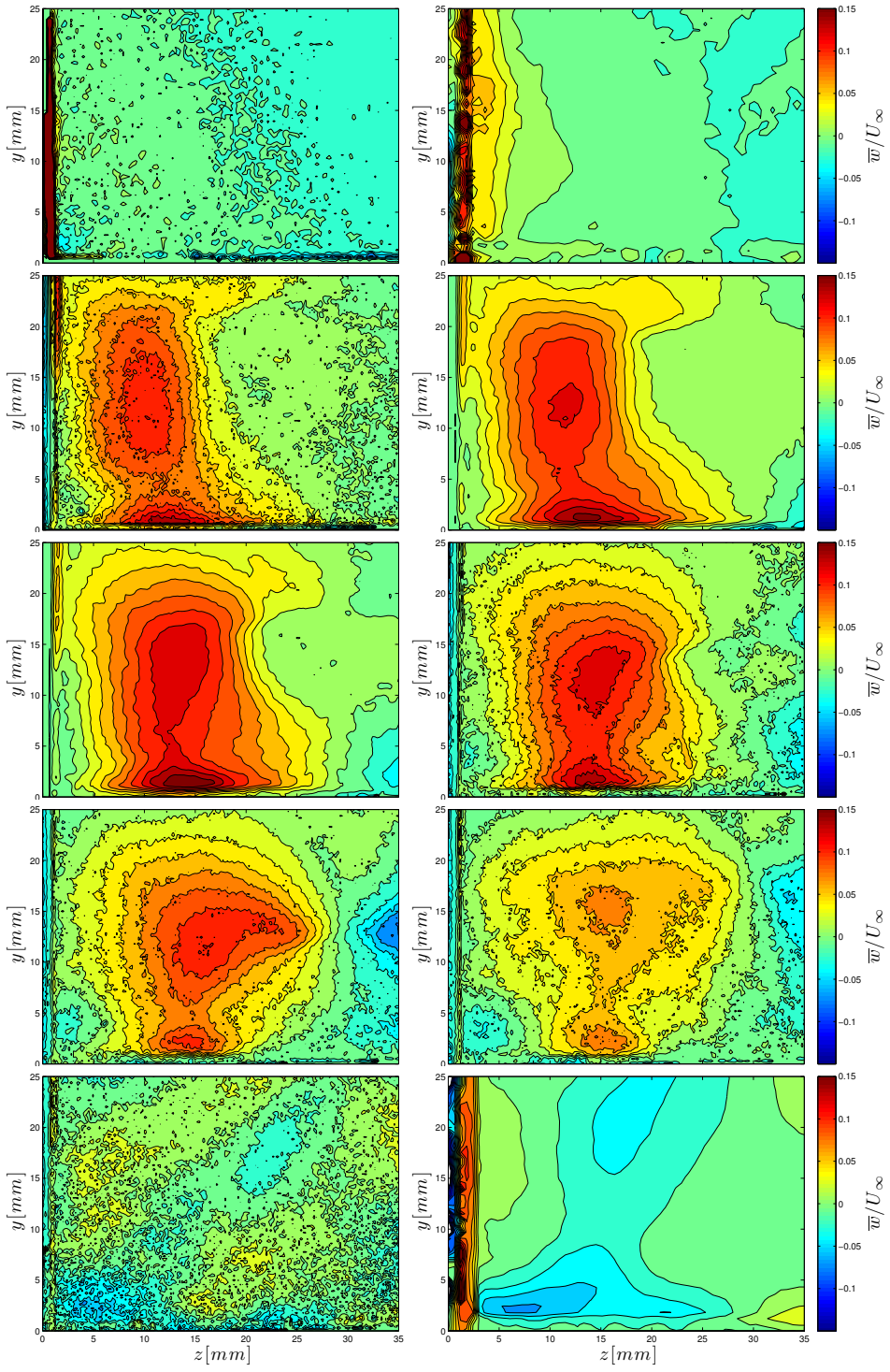

Figure D.3: Evolution of $\overline{v}/U_\infty$ through the SBLI - corner region for a flow deflection angle of $\theta = 6$–deg.

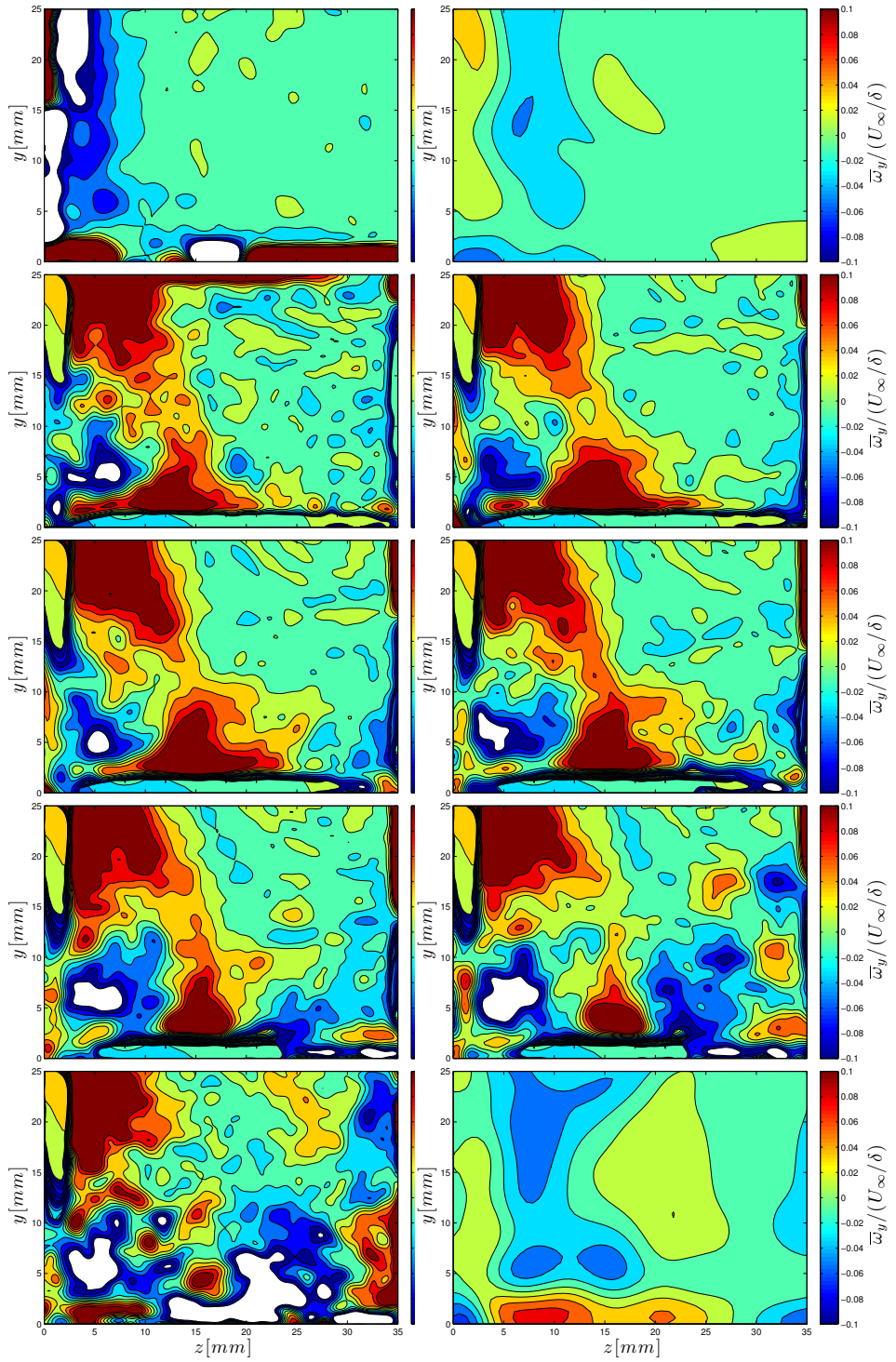

Figure D.4: Evolution of $\overline{\omega}_z/(U_\infty/\delta)$ through the SBLI - corner region for a flow deflection angle of $\theta = 6$–deg.

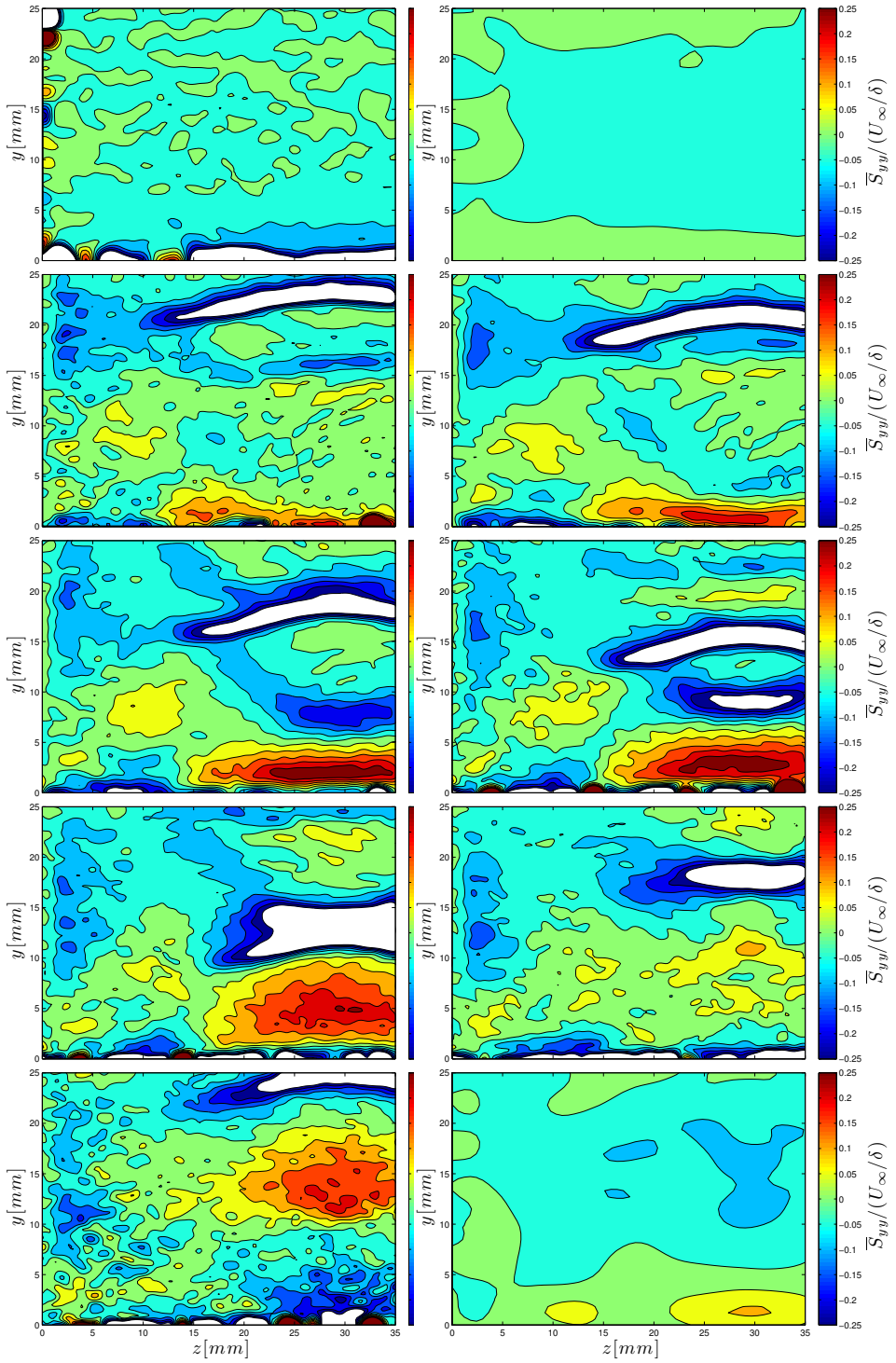

Figure D.5: Evolution of $\overline{S}_z z/(U_\infty/\delta)$ through the SBLI - corner region for a flow deflection angle of $\theta = 6$–deg.

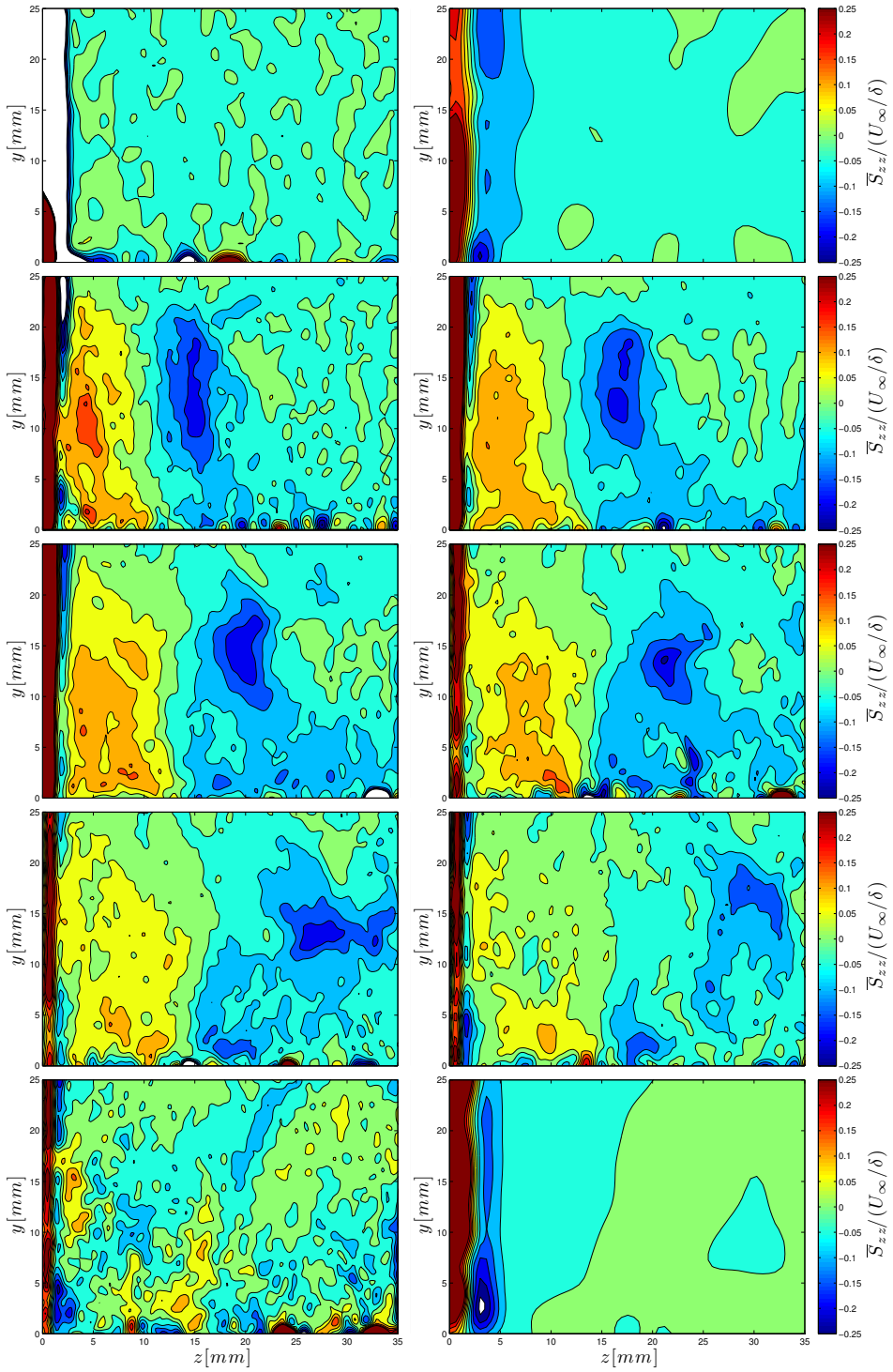

Figure D.6: Evolution of $\overline{S}_{zz}/(U_\infty/\delta)$ through the SBLI - corner region for a flow deflection angle of $\theta = 6$–deg.

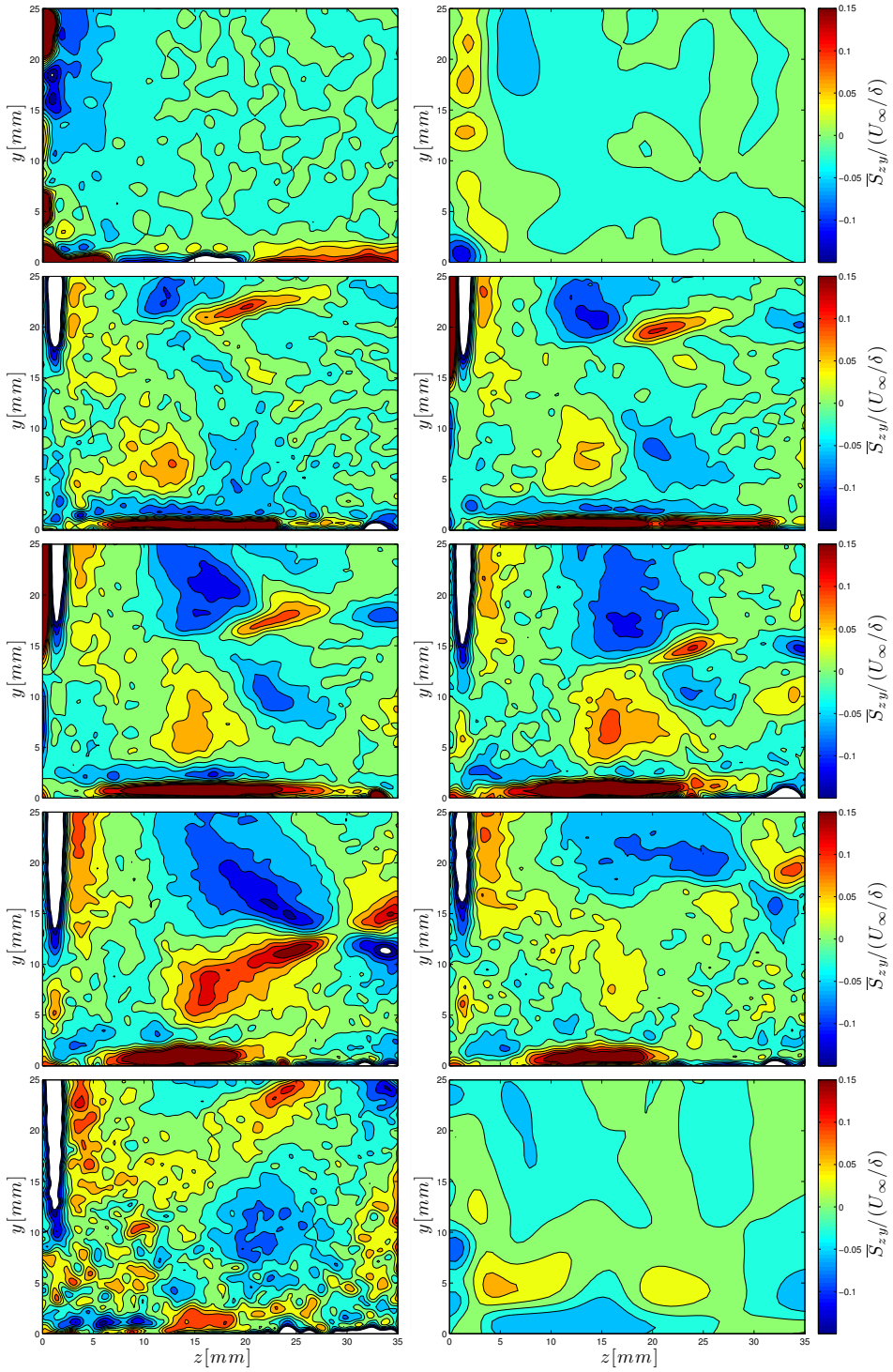

Figure D.7: Evolution of $\overline{S}_{xy}/(U_\infty/\delta)$ through the SBLI - corner region for a flow deflection angle of $\theta = 6$–deg.

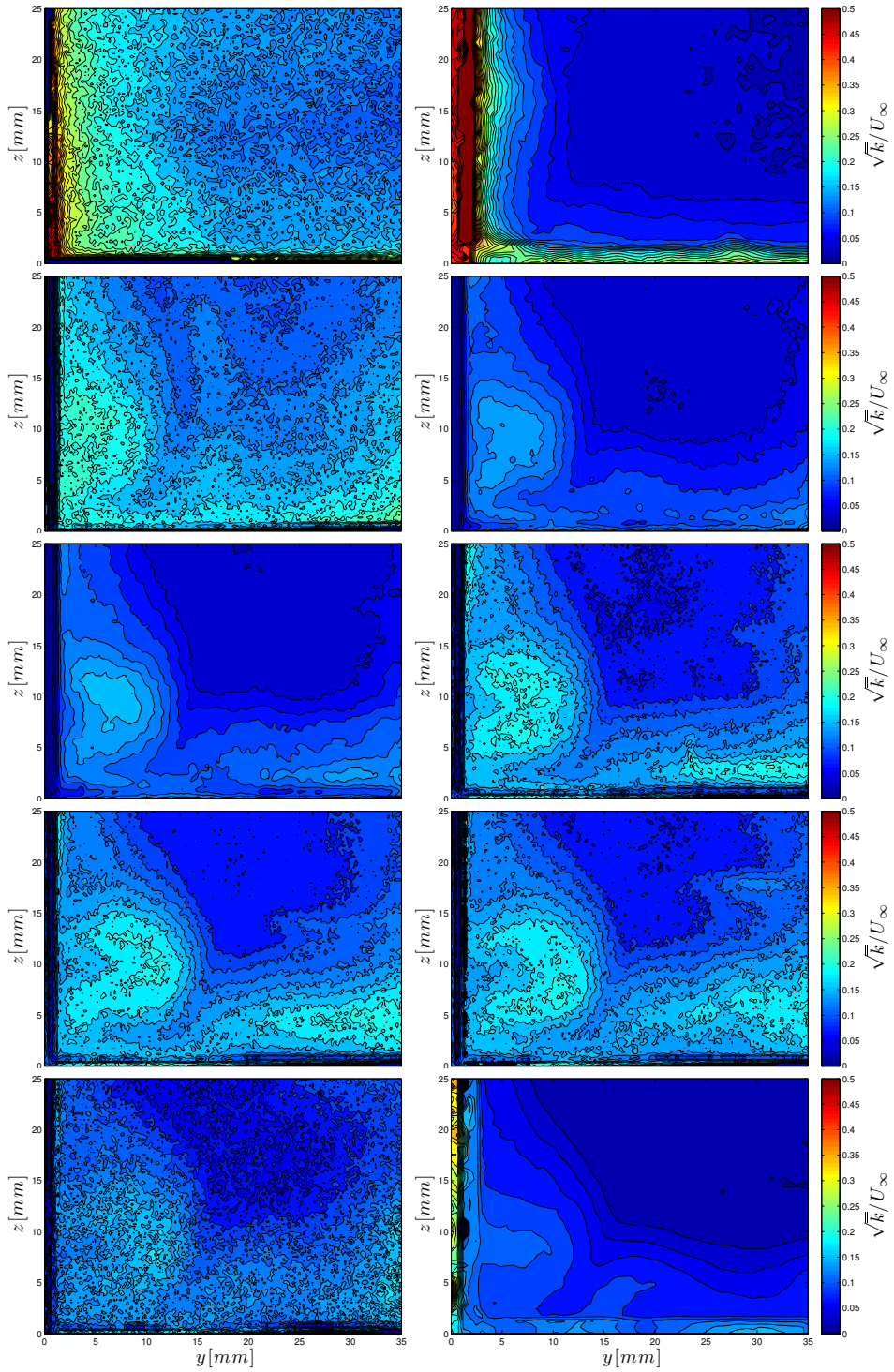

Figure D.8: Evolution of $\sqrt{\overline{k}}/U_\infty$ through the SBLI - corner region for a flow deflection angle of $\theta = 6$–deg.

BIBLIOGRAPHY

BIBLIOGRAPHY

Adamson Jr., T., Messiter, A., 1980. Analysis of two-dimensional interactions between shock waves and boundary layers. Annual Review of Fluid Mechanics 12 (1), 103–138.
URL http://www.annualreviews.org/doi/pdf/10.1146/annurev.fl.12.010180.000535

Adrian, R., Westerweel, J., 2010. Particle Image Velocimetry. Cambridge University Press, Cambridge.

Alizard, F., Rist, U., Robinet, J., 2009. Linear Instability of Streamwise Corner Flow. Advances in Turbulence XII, 67–70.
URL http://www.springerlink.com/index/q653713021852121.pdf

Alizard, F., Robinet, J., Rist, U., 2010. Sensitivity analysis of a streamwise corner flow. Physics of Fluids 22, 014103.
URL http://link.aip.org/link/?PHFLE6/22/014103/1

Alvi, F. S., Settles, G. S., 1992. Physical Model of the Swept Shock Wave / Boundary-Layer Interaction Flowfield. AIAA Journal 30 (9), 2252–2258.

Babinsky, H., Harvey, J. K., 2011. Shock Wave-Boundary-Layer Interactions. Cambridge Aerospace Series. Cambridge University Press.
URL http://books.google.com/books?id=3nIU5zS-94YC

Beresh, S. J., 1999. The effect of the incoming turbulent boundary layer on a shock-induced separated flow using particle image velocimetry. Ph.D. thesis, University of Texas at Austin.

Bookey, P., Wyckham, C., Smits, A., 2005. Experimental Investigations of Mach 3 Shock-Wave Turbulent Boundary Layer Interactions. AIAA Journal, 1–15.

Bottaro, A., Soueid, H., Galletti, B., 2006. Formation of secondary vortices in turbulent square-duct flow. AIAA Journal 44 (4), 803–811.
URL http://www.dicat.unige.it/bottaro/Papers/b-s-g.pdf

Bradshaw, P., 1987. Turbulent secondary flows. Annual Review of Fluid Mechanics 19, 53–74.

Bruce, P. J. K., Burton, D. M. F., Titchener, N. a., Babinsky, H., May 2011. Corner effect and separation in transonic channel flows. Journal of Fluid Mechanics 679, 247–262.
URL http://www.journals.cambridge.org/abstract_S0022112011001352

Cantwell, B. J., Jan. 1981. Organized Motion in Turbulent Flow. Annual Review of Fluid Mechanics 13 (1), 457–515.
URL http://www.annualreviews.org/doi/abs/10.1146/annurev.fl.13.010181.002325

Chapman, D. R., Kuehn, D. M., Larson, H. K., 1957. Investigation of separated flows in supersonic and subsonic streams with emphasis on the effect of transitions. Tech. rep., NACA Technical Note 3869.

Clemens, N., Mungal, M., May 1991. A planar Mie scattering technique for visualizing supersonic mixing flows. Experiments in Fluids 11-11 (2-3), 175–185.
URL http://www.springerlink.com/content/u62n5784712118j3/

Davis, D. O., Gessner, F. B., Aug. 1989. Further experiments on supersonic turbulent flow development in a square duct. AIAA Journal 27 (8), 1023–1030.
URL http://doi.aiaa.org/10.2514/3.10216

Debonis, J. R., Oberkampf, W. L., Consulting, W. L. O., Orkwis, P. D., Turner, M. G., Wolf, R. T., 2010. Assessment of CFD Models for Shock Boundary-Layer Interaction. Aerospace (July), 1–28.

Delery, J., Marvin, J. G., 1986. Shock-Wave Boundary Layer Interactions. Tech. Rep. 21.

Delery, J. M., Legendre, R., Werle, H., 2001. Toward the Elucidation of Three-Dimensional Separation. Annual Review of Fluid Mechanics 33, 129–154.

Derunov, E., Zheltovodov, A., Maksimov, A., 2008. Development of three-dimensional turbulent separation in the neighborhood of incident crossing shock waves. Thermophysics and Aeromechanics 15 (1), 29–54.
URL http://www.springerlink.com/index/VR71706XV2325128.pdf

Doerffer, P., Dallmann, U., 1987. Separation structures produced by normal shock-wave/turbulent boundary-layer interaction in a narrow wind tunnel. In: American Institute of Aeronautics and Astronautics Conference. p. 11.
URL http://adsabs.harvard.edu/abs/1987aiaa.confS....D

Dou, H.-S., Khoo, B. C., Yeo, K. S., Jul. 2006. Incipient separation in shock wave/boundary layer interactions as induced by sharp fin. Shock Waves 15 (6), 425–436.
URL http://www.springerlink.com/index/10.1007/s00193-006-0044-z

Dupont, P., Haddad, C., Ardissone, J., Debieve, J., Oct. 2005. Space and time organisation of a shock wave/turbulent boundary layer interaction. Aerospace Science

and Technology 9 (7), 561–572.
URL http://linkinghub.elsevier.com/retrieve/pii/S1270963805000593

Dupont, P., Piponniau, S., Sidorenko, A., Debieve, J. F., 2008. Investigation by Particle Image Velocimetry Measurements of Oblique Shock Reflection with Separation. AIAA Journal 46 (6), 6–11.

Dussauge, J., Dupont, P., Debieve, J., 2006. Unsteadiness in shock wave boundary layer interactions with separation. Aerospace Science and Technology 10 (2), 85–91.
URL http://linkinghub.elsevier.com/retrieve/pii/S1270963805001495

Eagle, W. E., Driscoll, J., Benek, J., 2011. Experimental Investigation of Corner Flows in Rectangular Supersonic Inlets with 3D Shock-Boundary Layer Effects . In: 49th AIAA Aerospace Sciences Meeting. AIAA, Orlando, FL.

Edwards, J., Aug. 2008. Numerical simulations of shock/boundary layer interactions using time-dependent modeling techniques: A survey of recent results. Progress in Aerospace Sciences 44 (6), 447–465.
URL http://linkinghub.elsevier.com/retrieve/pii/S0376042108000535

Elsinga, G. E., Adrian, R. J., Van Oudheusden, B. W., Scarano, F., Feb. 2010. Three-dimensional vortex organization in a high-Reynolds-number supersonic turbulent boundary layer. Journal of Fluid Mechanics 644, 35.
URL http://www.journals.cambridge.org/abstract_S0022112009992047

Fukuda, M. K., 1977. Bleed Effects on Shock / Boundary-Layer Interactions in Supersonic Mixed Compression Inlets 14 (2).

Gadd, G. E., Holder, D. W., Regan, J. D., 1954. An experimental investigation of the interaction between shock waves and boundary layers. Proceedings of the Royal Society of London. Series A, Mathematical and Physical Sciences 226 (1165), 227–253.

Ganapathisubramani, B., Clemens, N. T., Dolling, D. S., Road, P. C., Aug. 2007. Effects of upstream boundary layer on the unsteadiness of shock-induced separation. Journal of Fluid Mechanics 585, 369.
URL http://www.journals.cambridge.org/abstract_S0022112007006799

Garnier, E., 2009. Stimulated Detached Eddy Simulation of three-dimensional shock/boundary layer interaction. Shock Waves.
URL http://www.springerlink.com/content/7403057334133q51

Gessner, F. B., Jones, J. B., 1961. A Preliminary Study of Turbulence Characteristics of Flow Along a Corner. Journal of Basic Engineering, 657–662.
URL http://scholar.google.com/scholar?hl=en&btnG=Search&q=intitle:A+Prelimina

Ghia, K., 1975. Incompressible streamwise flow along an unbounded corner. AIAA Journal 13 (7), 902–907.
URL http://adsabs.harvard.edu/abs/1975AIAAJ..13..902G

Green, J., Jan. 1970. Interactions between shock waves and turbulent boundary layers. Progress in Aerospace Sciences 11, 235–340.
URL http://linkinghub.elsevier.com/retrieve/pii/0376042170900187

Hadjadj, A., Dussauge, J.-P., Nov. 2009. Shock wave boundary layer interaction. Shock Waves 19 (6), 449–452.
URL http://www.springerlink.com/index/10.1007/s00193-009-0238-2

Harloff, G. J., Smith, G. E., Apr. 1996. Supersonic-inlet boundary-layer bleed flow. AIAA Journal 34 (4), 778–785.
URL http://doi.aiaa.org/10.2514/3.13140

Helmer, D. B., 2011. Measurements of a three-dimensional shock-boundary layer interaction. Ph.D. thesis, Stanford University.

Hingst, W. R., Williams, K. E., 1991. Interaction of two glancing, crossing shock waves with a turbulent boundary-layer at various Mach numbers.

Hou, Y. X., Clemens, N. T., Dolling, D. S., 2003. Wide-Field PIV Study of Shock-Induced Turbulent Boundary Layer Separation. In: 41st AIAA Aerospace Sciences Meeting. No. January.

Humble, R. A., Elsinga, G. E., Scarano, F., Van Oudheusden, B. W., 2009. Three-dimensional instantaneous structure of a shock wave/turbulent boundary layer interaction. Journal of Fluid Mechanics 622 (1), 33.
URL http://www.journals.cambridge.org/abstract_S0022112008005090

Humble, R. a., Scarano, F., Oudheusden, B. W., Jun. 2007. Particle image velocimetry measurements of a shock wave/turbulent boundary layer interaction. Experiments in Fluids 43 (2-3), 173–183.
URL http://www.springerlink.com/index/10.1007/s00348-007-0337-8

Humble, R. A., Scarano, F., Oudheusden, B. W. V., Tuinstra, M., 2006. PIV Measurements of a Shock Wave / Turbulent Boundary Layer Interaction. In: 13th International Symposium on Applications of Laser Techniques to Fluid Mechanics. No. 1033.

Inger, G. R., Feb. 1987. Spanwise propagation of upstream influence in conical swept shock/boundary-layer interactions. AIAA Journal 25 (2), 287–293.
URL http://doi.aiaa.org/10.2514/3.9620

Ketchum, A. C., Bogdonoff, S. M., Fernando, E. M., Batcho, P. F., 1989. Preliminary study of the interactions caused by crossing shock waves and a turbulent boundary layer.

Knight, D. D., Garrison, T. J., Settles, G. S., Zheltovodov, A. A., Maksimov, A. I., Shevchenko, A. M., Vorontsov, S. S., 1995. Asymmetric Crossing-Shock-Wave/Turbulent-Boundary-Layer Interaction. AIAA Journal 33 (12).

Knight, D. D., Horstman, C. C., Bogdonoff, S., Shapey, B., 1986. The flowfield structure of the 3-D shock wave-Boundary layer interaction generated by a 20 deg sharp fin at Mach 3. In: 24th AIAA Aerospace Sciences Meeting. p. 16.
URL http://www.aric.or.kr/treatise/journal/content.asp?idx=56363

Korkegi, R. H., 1973. A Simple Correlation for Incipient Turbulent Boundary-Layer Separation due to a Skewed Shock Wave. AIAA Journal 11 (11), 1578–1579.

Korkegi, R. H., Apr. 1975. Comparison of Shock-Induced Two- and Three- Dimensional Incipient Turbulent Seperation. AIAA Journal 13 (4), 534–535.
URL http://doi.aiaa.org/10.2514/3.49750

Kubota, H., Stollery, J. L., 1982. An experimental study of the interaction between a glancing shock wave and a turbulent boundary layer. Journal of Fluid Mechanics 116, 431–458.
URL href="http://dx.doi.org/10.1017/S0022112082000548

Lapsa, A. P., 2009. Experimental Study of Passive Ramps for Control of Shock Boundary Layer Interactions. Ph.D. thesis, University of Michigan.

Lapsa, A. P., Dahm, W. J. a., Jun. 2010. Stereo particle image velocimetry of nonequilibrium turbulence relaxation in a supersonic boundary layer. Experiments in Fluids 50 (1), 89–108.
URL http://www.springerlink.com/index/10.1007/s00348-010-0897-x

Lawson, N. J., Wu, J., 1997. Three-dimensional particle image velocimetry : error analysis of stereoscopic techniques. Measurement Science and Technology 8 (8), 894–900.

Legendre, R., 1956. Separation de courant l'ecoulement laminarire tridimnesionnel. Rech. Aero, 3–8.

Libby, P., 1966. Secondary flows associated with a supersonic corner region(Secondary flow for supersonic boundary layers with or without swept edges, noting effect of compressibility and heat transfer on reverse flow). AIAA JOURNAL 4 (6), 1130–1132.
URL http://www.csa.com/partners/viewrecord.php?requester=gs&collection=TR

Loitsianskii, L., Bolshakov, V., NACA, 1951. On motion of fluid in boundary layer near line of intersection of two planes. Tech. rep., NACA Technical Memo 1308.
URL http://scholar.google.com/scholar?hl=en&btnG=Search&q=intitle:On+motion+o

Louis, J., van Oudheusden, B., Scarano, F., Dupont, P., 2008. Unsteadiness Characterization in a Shock Wave Turbulent Boundary Layer Interaction through Dual-PIV. In: 38th Aerospace Sciences Meeting. No. June. pp. 1–13.
URL http://www.aric.or.kr/treatise/journal/content.asp?idx=106823

Lu, F., 1983. An Experimental Study of Three-Dimensional Shock-Wave Boundary Layer Interactions Generated by Sharp Fins. NASA CR 170107, 1–165.

Lu, F., 2010. Surface oil flow visualization. The European Physical Journal-Special Topics 182 (1), 51–63.
URL http://www.springerlink.com/index/VJ537018V68587QP.pdf

Lu, F. K., Apr. 1993. Quasiconical free interaction between a swept shock and a turbulent boundary layer. AIAA Journal 31 (4), 686–692.
URL http://doi.aiaa.org/10.2514/3.11604

Lu, F. K., Settles, G. S., 1990. Color surface-flow visualization of fin-generated shock wave boundary-layer interactions. Experiments in Fluids 8 (6), 352{–}354.

Lu, F. K., Settles, G. S., May 1991. Inception length to a fully developed, fin-generated, shock-wave, boundary-layer interaction. AIAA Journal 29 (5), 758–762.
URL http://doi.aiaa.org/10.2514/3.10651

Mee, D. J., Stalker, R. J., Stollery, J. L., 1986. Glancing interactions between single and intersecting oblique shock waves and a turbulent boundary layer. Journal of Fluid Mechanics 170, 411–433.
URL href="http://dx.doi.org/10.1017/S0022112086000952

Mitchell, D., Honnery, D., Soria, J., May 2011. Particle relaxation and its influence on the particle image velocimetry cross-correlation function. Experiments in Fluids 51 (4), 933–947.
URL http://www.springerlink.com/index/10.1007/s00348-011-1116-0

Moffatt, H. K., Tsinober, A., Mechanics, I. U. o. T., Applied, 1990. Topological fluid mechanics: proceedings of the IUTAM Symposium, Cambridge, UK, 13-18 August 1989. Cambridge University Press.
URL http://books.google.com/books?id=X6Csp76ka2sC

Mojola, O. O., 1976. Steady flow separation along a straight streamwise corner. Applied Science Research (1).

Muppidi, S., Mahesh, K., 2007. DNS of unsteady shock boundary layer interaction. AIAA, 1–18.
URL http://www.advising.it.umn.edu/people/faculty/mahesh/publpdf/conference/s

Narayanswami, N., Knight, D. D., Bogdonoff, S. M., Horstman, C. C., 1991. Crossing shock wave-turbulent boundary layer interactions.

Perry, A. E., Chong, M. S., 1987. A Description of Edding Motions and Flow Patterns Using Critical-Point Concepts. Annual Review of Fluid Mechanics 19, 125–155.

Pirozzoli, S., Grasso, F., 2006. Direct numerical simulation of impinging shock wave/turbulent boundary layer interaction at M=2.25. Physics of Fluids 18 (6), 065113.
URL http://link.aip.org/link/PHFLE6/v18/i6/p065113/s1&Agg=doi

Reda, D. C., Murphy, J. D., Feb. 1973a. Shock Wave/Turbulent Boundary-Layer Interactions in Rectangular Channels. AIAA Journal 11 (2), 139–140.
URL http://doi.aiaa.org/10.2514/3.50592 http://doi.aiaa.org/10.2514/3.50445

Reda, D. C., Murphy, J. D., Oct. 1973b. Sidewall Boundary-Layer Influence on Shock Wave/Turbulent Boundary-Layer Interactions. AIAA Journal 11 (10), 139–140.
URL http://doi.aiaa.org/10.2514/3.50592 http://doi.aiaa.org/10.2514/3.50445

Ringuette, M. J., Wu, M., Martín, M. P., Quad, E., St, O., Dec. 2007. Coherent structures in direct numerical simulation of turbulent boundary layers at Mach 3. Journal of Fluid Mechanics 594, 59–69.
URL http://www.journals.cambridge.org/abstract_S0022112007009020

Samimy, M., Lele, S. K., Aug. 1991. Motion of particles with inertia in a compressible free shear layer. Physics of Fluids A: Fluid Dynamics 3 (8), 1915.
URL http://link.aip.org/link/?PFADEB/3/1915/1

Schmisseur, J. D., Dolling, D. S., 1992. Unsteady separation in sharp fin-induced shock wave/turbulent boundary layer interaction at Mach 5.

Settles, G., Dodson, L., 1994. Hypersonic Shock/Boundary-Layer Interaction Database: New and Corrected Data, NASA-CR 177638, April 1994. Tech. Rep. April 1994, Department of Mechanical Engineering, Penn State University, University Park, PA.
URL http://scholar.google.com/scholar?hl=en&btnG=Search&q=intitle:Hypersonic+

Squire, L. C., 1961. The motion of a thin oil sheet under the steady boundary layer on a body. Journal of Fluid Mechanics 11 (02), 161–179.
URL href="http://dx.doi.org/10.1017/S0022112061000445

Tabak, M., Peake, D. J., 1982. Topology of Three-Dimensional Separated Flows. Annual Review of Fluid Mechanics 14, 61–85.

Urban, W. D., Mungal, M. G., 1998. A PIV study of compressible shear layers. Ninth International Symposium on Application of Laser Techniques to Fluid Mechanics.

Watson, R., Weinstein, L., 1971. A study of hypersonic corner flow interactions. AIAA Journal 9, 1280–1286.
URL http://adsabs.harvard.edu/abs/1971AIAAJ...9.1280W

Wedin, H., Bottaro, A., Nagata, M., 2009. Nonlinear coherent structures in a square duct. Advances in Turbulence XII, 141–144.
URL http://www.springerlink.com/index/h10342674224v35u.pdf

Wu, M., Martin, M. P., Apr. 2007. Direct Numerical Simulation of Supersonic Turbulent Boundary Layer over a Compression Ramp. AIAA Journal 45 (4), 879–889.
URL http://doi.aiaa.org/10.2514/1.27021

Zheltovodov, A., Maksimov, A., Schulein, E., Knight, D., Thivet, F., Gaitonde, D., Schmisseur, J., 2001. Experimental and computational studies of crossing-shock-wave/turbulent-boundary-layer interactions. In: Proceedings of the International Conference on Recent Developments in Applied Mathematics and Mechanics. Vol. 1560. pp. 153–162.
URL http://www.sbras.ru/ws/NikNik/1617/rep1617.pdf